Global Biogeochemical Cycles®

RESEARCH ARTICLE
10.1029/2022GB007347

Key Points:

- An aquatic phosphorus module was incorporated into a land biosphere model to investigate phosphorus dynamics along the land-ocean continuum
- Simulated riverine exports of dissolved inorganic phosphorus, dissolved organic phosphorus, particulate inorganic phosphorus, and particulate organic phosphorus from the Mississippi River Basin increased remarkably during 1901–2018
- The growing use of fertilizer and intensified soil erosion were the primary reasons for the increasing phosphorus exports

Supporting Information:

Supporting Information may be found in the online version of this article.

Correspondence to:

H. Tian,
tianhan@auburn.edu

Citation:

Bian, Z., Pan, S., Wang, Z., Yao, Y., Xu, R., Shi, H., et al. (2022). A century-long trajectory of phosphorus loading and export from Mississippi River Basin to the Gulf of Mexico: Contributions of multiple environmental changes. *Global Biogeochemical Cycles*, *36*, e2022GB007347. https://doi.org/10.1029/2022GB007347

Received 6 FEB 2022
Accepted 24 MAY 2022

A Century-Long Trajectory of Phosphorus Loading and Export From Mississippi River Basin to the Gulf of Mexico: Contributions of Multiple Environmental Changes

Zihao Bian[1], Shufen Pan[1], Zhuonan Wang[1], Yuanzhi Yao[1], Rongting Xu[1,2], Hao Shi[1], Latif Kalin[1], Christopher Anderson[1], Dubravko Justic[3], Steven Lohrenz[4], and Hanqin Tian[1]

[1]International Center for Climate and Global Change Research, and College of Forestry, Wildlife and Environment, Auburn University, Auburn, AL, USA, [2]Forest Ecosystems and Society, Oregon State University, Corvallis, OR, USA, [3]College of the Coast and Environment, Louisiana State University, Baton Rouge, LA, USA, [4]School for Marine Science and Technology, University of Massachusetts Dartmouth, New Bedford, MA, USA

Abstract Phosphorus (P) control is critical to mitigating eutrophication in aquatic ecosystems, but the effectiveness of controlling P export from soils has been limited by our poor understanding of P dynamics along the land-ocean aquatic continuum as well as the lack of well-developed process models that effectively couple terrestrial and aquatic biogeochemical P processes. Here, we coupled riverine P biogeochemical processes and water transport with terrestrial processes within the framework of the Dynamic Land Ecosystem Model to assess how multiple environmental changes, including fertilizer and manure P uses, land use, climate, and atmospheric CO_2, have affected the long-term dynamics of P loading and export from the Mississippi River Basin to the Gulf of Mexico during 1901–2018. Simulations show that riverine exports of dissolved inorganic phosphorus (DIP), dissolved organic phosphorus, particulate organic phosphorus (POP), and particulate inorganic phosphorus (PIP) increased by 42%, 53%, 60%, and 53%, respectively, since the 1960s. Riverine DIP and PIP exports were the dominant components of the total P flux. DIP export was mainly enhanced by the growing mineral P fertilizer use in croplands, while increased PIP and POP exports were a result of the intensified soil erosion due to increased precipitation. Climate variability resulted in substantial interannual and decadal variations in P loading and export. Soil legacy P continues to contribute to P loading. Our findings highlight the necessity to adopt effective P management strategies to control P losses through reductions in soil erosion, and additionally, to improve P use efficiency in crop production.

Plain Language Summary Phosphorus enrichment in aquatic systems is one of the critical reasons for water quality degradation. Terrestrial ecosystems have received large amounts of phosphorus inputs and are a major phosphorus source for water bodies. Linking the phosphorus cycles in both terrestrial and aquatic ecosystems is helpful for understanding phosphorus flux from land to ocean. In this study, we simulated phosphorus processes in both terrestrial and aquatic systems and estimated phosphorus exports from the Mississippi River Basin to the Gulf of Mexico during 1901–2018. The simulated results show that riverine phosphorus exports have increased since the 1960s. The increasing usage of fertilizer and manure in agricultural activities as well as intensified erosion due to increasing extreme precipitation could be the major causes for the increasing riverine phosphorus export. This study provides insight into the mechanisms mediating riverine phosphorus exports over the past century in the context of global change.

1. Introduction

Since the middle of the twentieth century, a substantial amount of geological phosphorus (P) has entered terrestrial ecosystems as fertilizer to stimulate crop production (Elser & Bennett, 2011). Global mobilization of P has roughly tripled compared to its natural state (Smil, 2000) and the riverine P flux from land to ocean has accelerated (Carpenter, 2005). As the P cycle is a largely one-way flow from rock to soil and finally to streams, lakes, and oceans, the growing use of industrial P fertilizer is rapidly depleting the supply of mineable deposits of P rock which are in limited supply and unevenly distributed around the world (Amundson et al., 2015). Furthermore, the increasing amount of P entering water bodies can disturb the ecological balance of aquatic systems, cause eutrophication and water quality degradation, and threaten human health and economic activities (Garnier

et al., 2015). Freshwater lakes, reservoirs, and streams are typically P limited and vulnerable to P enrichment (Colborne et al., 2019; Correll, 1998). While coastal and oceanic hypoxia is commonly associated with nitrogen (N) loading (Ryther & Dunstan, 1971), the impact of P on coastal areas can also be detrimental to the headwaters of estuaries (Correll, 1998) and coastal areas with historically excessive nutrient loading (Conley et al., 2009; Lohrenz et al., 2008). The increasing loading of N, relative to P, from the Mississippi River Basin (MRB) has been associated with periodic P limitation in river-influenced regions of the northern Gulf of Mexico, especially during the spring bloom period (Sylvan et al., 2007). As studies suggest the important role of P in the occurrence of Gulf hypoxia, there is a growing recognition of the need to control both N and P loading from the MRB (Fennel & Laurent, 2018; Scavia & Donnelly, 2007; Sylvan et al., 2006). Therefore, evaluating P loading and export from land to ocean is critical for sustainable nutrient management and water security.

Numerous statistical and mechanistic models have been used to estimate P losses from terrestrial ecosystems to waterways. The net anthropogenic phosphorus inputs method is a classic statistical approach to link terrestrial water and nutrient budgets to water quality (Hu et al., 2020; Metson et al., 2017). Watershed models have been developed to simulate distributed landscape P generation by combining statistical and mechanistic approaches. However, terrestrial P cycling processes are still over-simplified in these watershed models compared with terrestrial biogeochemical models. Specifically, P pools and fluxes related to weathering, adsorption/desorption, occlusion, and biological turnover are not fully and explicitly represented in most watershed models or global models (Harrison et al., 2019). As a result, these models can only simulate the loading of a limited number of P species. Total P (TP) load is the only variable that can be simulated in many watershed models, for example, the SPARROW and the IMAGE–GNM models (Alexander et al., 2008; Beusen et al., 2015). In contrast, terrestrial biogeochemical models are capable of simulating a relatively complete P cycle in terrestrial ecosystems, as well as investigating the effects of multiple environmental factors on P fluxes and pools over long time scales (Goll et al., 2017; Wang et al., 2020; Yang et al., 2013).

In-stream P processes within many watershed models have generally only considered P retention, while the interactions between various P components have often been neglected (Robson, 2014). Phosphorus flux to aquatic ecosystems is strongly influenced by climate, land-use condition, and soil P concentration in terrestrial ecosystems (Bennett et al., 2001). Riverine biogeochemical and physical processes during riverine transport also matter, especially for large basins where the residence time of P inside rivers is longer than the time-scale of in-channel P transformation (Ruttenberg, 2003). Different from watershed models, aquatic P models often incorporate more P components and complex biogeochemical processes (Robson, 2014). For example, the RIVE and CE–QUAL–W2 models are capable of simulating P transfers and stocks of various forms between abiotic environment, organic matter, and inorganic matter (Aissa-Grouz et al., 2018; Cole & Wells, 2006). Nevertheless, aquatic P models usually rely on accurate boundary conditions determined from water samples or land inputs. The gap between a single P variable (e.g., TP) output from watershed models and multiple P variables in the boundary condition required by aquatic models can create difficulties when trying to link two different types of models (Debele et al., 2008). In contrast, terrestrial biogeochemical models usually incorporate several P variables and can provide detailed boundary information for aquatic models. Therefore, it will be much helpful to couple the terrestrial P cycle, including soil, plant, and microbial processes, with the P cycle in aquatic ecosystems for understanding the P dynamics along the terrestrial–aquatic continuum.

However, models that can comprehensively couple P processes across the land–aquatic interface are still lacking. In particular, previous studies based on limited observational data and over-simplified models have not adequately addressed how climate and human activities could interactively impact P export at a century-long time scale (Alexander et al., 2008; Stackpoole et al., 2021). Connecting P transformation and transport between the terrestrial and aquatic ecosystems can provide a new perspective to evaluate the P dynamic along the terrestrial-aquatic continuum and its response to environmental changes. Here, we intend to link P cycles across terrestrial and aquatic ecosystems by developing an aquatic P module within the framework of the Dynamic Land Ecosystem Model (DLEM). DLEM (the C and N coupled version) has been applied to investigate riverine exports of C and N from the MRB and the Chesapeake Bay Watershed (Pan et al., 2021; Ren et al., 2016; Tian, Ren, et al., 2015; Tian et al., 2020; Yao et al., 2021) and has recently been updated to include terrestrial P processes (Wang et al., 2020). In this study, our objectives were to (a) describe our efforts to incorporate the biogeochemical processes of riverine P dynamics and a water transport module into DLEM; (b) use the MRB as a testbed to evaluate the performance of the improved DLEM in simulating P loading and export across the land–aquatic

interface, (c) estimate the exports of dissolved inorganic phosphorus (DIP), dissolved organic phosphorus (DOP), particulate organic phosphorus (POP), and particulate inorganic phosphorus (PIP) from the MRB to the Gulf of Mexico during 1901–2018; and (d) further quantify the contributions of climate, anthropogenic P input, land-use change (LUC), and atmospheric CO_2 concentration to changes in P loading over the study period. This work will improve our understanding of underlying mechanisms controlling P loading and provide valuable information for nutrient management and pollution mitigation in the MRB.

2. Model and Data

2.1. Integrated Modeling of Terrestrial–Aquatic Processes

DLEM is a process-based model coupling terrestrial biophysics, plant phenology, soil biogeochemistry, and vegetation dynamics (Pan et al., 2015, 2020; Tian et al., 2010, 2015). The model is capable of simulating biogeochemical and hydrological cycles across the soil–plant–atmosphere continuum. Recently, we have coupled the P processes and C–N–P interactions into the DLEM and established the DLEM–CNP modeling scheme where the C, N, and P cycles are fully coupled through photosynthesis, allocation, turnover, nutrient uptake, and decomposition (Figure S1a in Supporting Information S1) (Wang et al., 2020). Other land P processes in the DLEM–CNP include weathering from the mineral P pool, adsorption and desorption between the labile P pool and the secondary mineral P pool, and occlusion of the secondary mineral P to the occluded P pool (Figure S1b and Text S1 in Supporting Information S1). Simultaneously, to evaluate and predict biogeochemical dynamics along the terrestrial–aquatic continuum, we have incorporated river C and N cycling into the DLEM and established a Terrestrial/Aquatic scheme (Liu et al., 2013; Ren et al., 2016; Tao et al., 2014; Tian et al., 2015, 2020). In the most recent version of the DLEM–Terrestrial/Aquatic scheme, a scale-adaptive river transport module was incorporated and the hydrological processes were improved (Yao et al., 2020, 2021). The land component in the DLEM–CNP calculates soil erosion and P leaching, which can act as forcing factors in the aquatic module. In this study, we developed a model representation of riverine P dynamics in the DLEM–Terrestrial/Aquatic scheme and connected it to the land component of the DLEM–CNP, which further enhances modeling ability for simulating CNP cycling along the terrestrial–aquatic continuum.

2.2. P Yields From Terrestrial Ecosystems

Phosphorus yields from terrestrial ecosystems include DIP, DOP, POP, and PIP (Figure 1). DIP is derived from the labile P pool and enters aquatic systems through leaching and runoff. Similarly, DOP is the dissolved organic form of P, and can be leached out of soil through surface or subsurface runoff. Both POP and PIP enter into aquatic systems through soil erosion during runoff generation processes. POP is derived from the organic matter pool while PIP is derived from the mineral P pool, the secondary mineral P pool, and the occluded P pool. Daily Y_x (g P m^{-2}), yield of constituent x (DIP and DOP), in each grid is calculated as:

$$Y_{DIP} = SLP \cdot \frac{Q}{Q+W} / b_{DIP} \quad (1)$$

$$Y_{DOP} = DOP \cdot \frac{Q}{Q+W} \quad (2)$$

where SLP and DOP represent soil labile P and dissolved organic P pools (g P m^{-2}), respectively; Q is daily water yield (surface runoff and subsurface runoff) (mm) of the terrestrial ecosystem and W is the soil water content (mm) in the surface layer (0.5 m); b_{DIP} is the parameter controlling the adsorption capacity of soil for labile P (unitless). Yields of POP and PIP are as follows:

$$Y_{POP} = E \cdot C_{POP} \quad (3)$$

$$Y_{PIP} = E \cdot (C_{MP} + C_{SMP} + C_{OP}) \quad (4)$$

where C_{POP}, C_{MP}, C_{SMP}, *and* C_{OP} represents the concentration of total organic P, mineral P, secondary mineral P, and occluded P in the surface soil column (g P g^{-1} soil); E is the daily sediment yield due to soil erosion (g soil m^{-2}) and was calculated according to the Modified Universal Soil Loss Equation (MUSLE) (Neitsch et al., 2011; Williams, 1995).

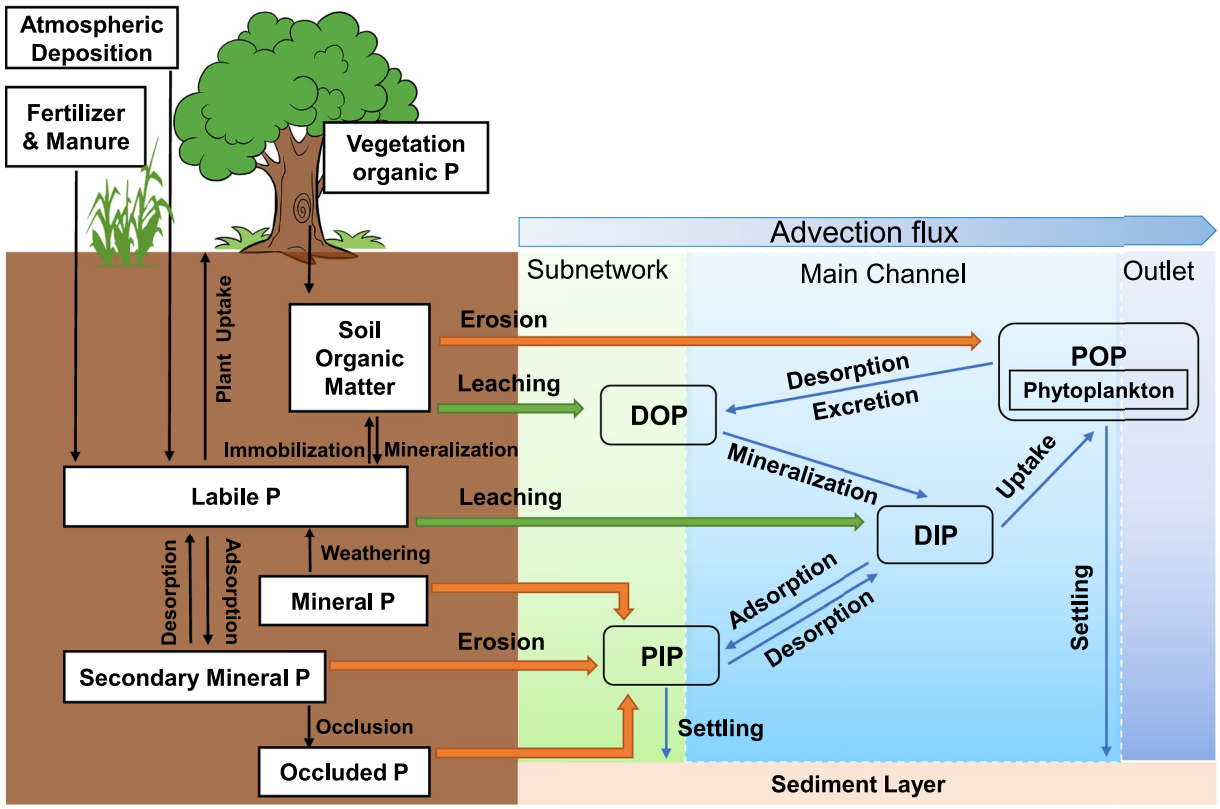

Figure 1. The coupled terrestrial and aquatic P cycling processes in the Dynamic Land Ecosystem Model–Terrestrial/Aquatic scheme. The pools and fluxes inside soil and vegetation (left side) are terrestrial component and the pools and fluxes inside water (right side) are aquatic component developed in this study.

$$E = a \cdot (Q \cdot q_{peak} \cdot area)^{b} \cdot K_{USLE} \cdot C_{USLE} \cdot P_{USLE} \cdot LS_{USLE} \cdot CFRG \quad (5)$$

where q_{peak} is daily peak runoff rate ($m^3\ s^{-1}$) and *area* is the land area (ha) within the grid (we assumed each grid represents a hydrological unit; Tesfa et al., 2014); K_{USLE}, C_{USLE}, P_{USLE}, LS_{USLE} represent factors for soil erodibility, cover and management, support practice, and topography, respectively; *CFRG* is the course fragment factor; *a* and *b* are the fit coefficients in the equation.

The wastewater P discharge in each grid cell is estimated based on an empirical approach developed by Van Drecht et al. (2009). The wastewater P mainly consists of P in human waste, laundry detergents, and dishwasher detergents, which are calculated as:

$$SWP_{i,y} = Pop_{i,y}\,(Hum_{i,y} + Det_{y})\,D_{y}\,(1 - R_{y}) \quad (6)$$

where $SWP_{i,y}$ is the wastewater P discharge to surface water from sewage (g P $person^{-1}$ day^{-1}) in year *y* and grid cell *i*; $Pop_{i,y}$ is population (person); $Hum_{i,y}$ and Det_{y} (g P $person^{-1}$ day^{-1}) are wastewater P from human excreta and P-based detergents (laundry and dishwater), respectively; D_{y} is the fraction of the total population that is connected to public sewage systems and R_{y} is the removal fraction of P through wastewater treatment. The large-scale usage of P-based detergents started in 1940 when synthetic detergents were newly introduced, and the banning of phosphates in detergents emerged in the early 1970s, which culminated in a nationwide voluntary ban in 1994 (Litke, 1999). The peak value of detergent P usage in 1970 was estimated as 0.82 g P $person^{-1}$ day^{-1} (Van Drecht et al., 2009), and we assumed it linearly increased from 1940 to 1970 then linearly decreased until 1994. The fraction of households connected to sewage systems in the U.S. was around 75% after 2000 (van Puijenbroek et al., 2019). The construction of sewage systems in industrialized countries started from the year 1870 onward, and a linear increase in D_{y} could be assumed for the period 1870–2000 (Morée et al., 2013). The general P removal fractions of primary treatment, secondary treatment, and tertiary treatment were estimated as 10%, 45%, and 90%, respectively (Van Drecht et al., 2009). The large-scale secondary treatment in the U.S. began around

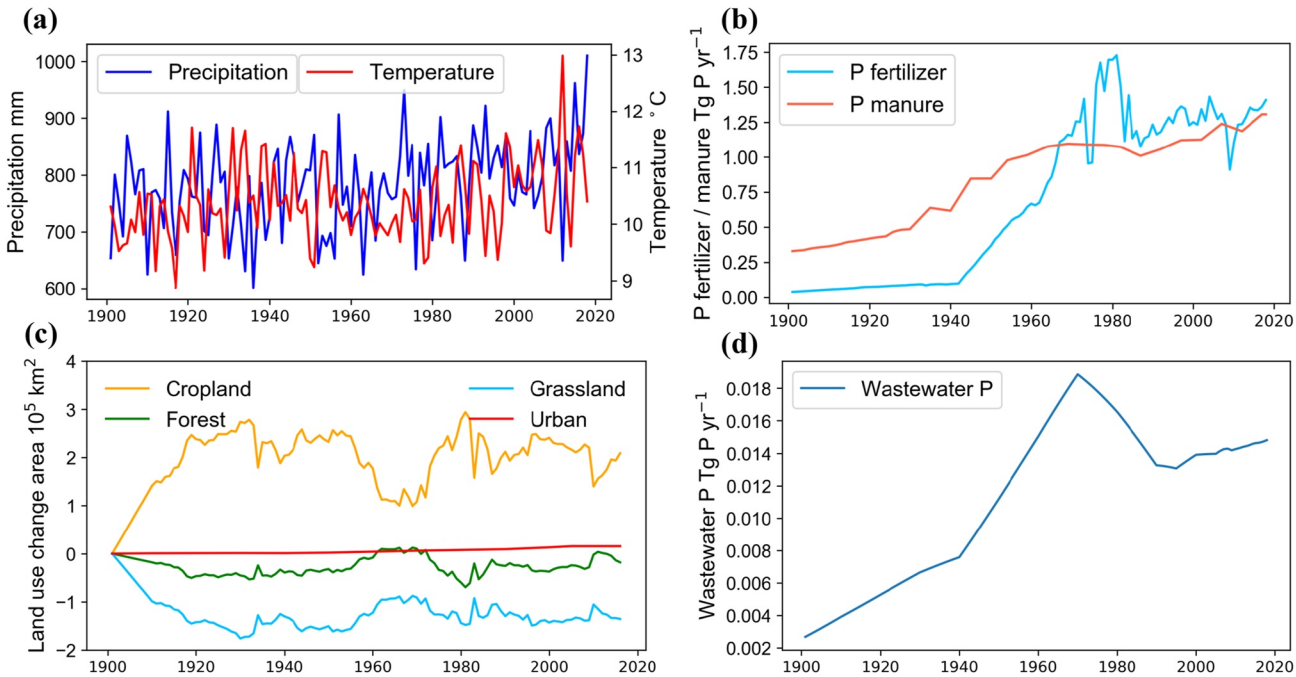

Figure 2. Interannual variation of (a) climate, (b) fertilizer and manure P inputs, (c) land-use change area, and (d) wastewater P in the Mississippi River Basin.

1920 and tertiary treatment started to grow rapidly since 1970 (Hale et al., 2015). Thus we assumed R_y value were linearly increased to 0.1 in 1920, and to 0.45 in 1970, then it increased at a rate of 0.9% per year until 1990, and 0.3% afterwards according to the change rate of R estimated by Van Drecht et al. (2009). *Hum* was calculated as:

$$Hum_{i,y} = HumN_{i,y} f_{NP} \tag{7}$$

$$HumN_{i,y} = 0.365 \left[4 + 14 \left(\frac{GDP_{i,y}}{33,000} \right)^{0.3} \right] \tag{8}$$

where $HumN_{i,y}$ is the protein N intake (g N person^{-1} day^{-1}) and is estimated according to empirical relationships with per capita gross domestic product (GDP) (Van Drecht et al., 2009); f_{NP} is the ratio between human P and human N intake and set as 1:10 (mass basis) (Morée et al., 2013). The TP estimated in this approach is divided into DIP (57.0%), DOP (0.5%), POP (2.3%), and PIP (40.2%) according to the information provided by Gu et al. (2011). The wastewater P directly enters surface water within each grid, and the simulated total wastewater P is presented in Figure 2d.

2.3. Advective P Flux

The aquatic module of the DLEM–Terrestrial/Aquatic scheme consists of physical transport processes and biochemical processes in inland water systems. The physical transport processes are designed based on a scale-adaptive water transport scheme (Model of Scale Adaptive River Transport (MOSART) (Li et al., 2013). The channel routine processes within a grid cell are separated into three unique parts, namely hillslope flow, subnetwork flow, and main-channel flow (Figure S2 in Supporting Information S1). Hillslope flow and subsurface runoff receive water and C, N, P yields from terrestrial ecosystems, and converge as subnetwork flow. Then local subnetwork flow combined with upstream water drains into the main-channel and the main-channel flow drains into the downstream grid-cell. Through parameterization (such as flow length, channel slope, and surface roughness) using aggregated high-resolution topography and river network data, the MOSART model can work in a scale-adaptive way. This feature of MOSART allows our aquatic module to operate at a relatively coarse spatial resolution but without a decrease in the simulation accuracy. The DLEM–Terrestrial/Aquatic scheme

coupled with MOSART hydrological module has been applied to quantify the C and N loading and performed well (Pan et al., 2021; Yao et al., 2021).

The transport rates of P in the subnetwork flow and the main channel flow are consistent with water transport. The Kinematic Wave Method, a simplified version of Saint-Venant equations that ignores backwater effects, was introduced to calculate water transport in the model (Chow, 2010), which is given as:

$$\begin{cases} \dfrac{\partial Q}{\partial x} + B\dfrac{\partial h}{\partial t} = q \\ S_f - S_0 = 0 \end{cases} \tag{9}$$

where Q is outflow rate ($m^3\ s^{-1}$); x is the direction of flow; h is the depth of river channel (m) and B is the width of the river channel (m) (we assumed the channel is rectangular); q is lateral inflow from subnetwork or main channel ($m^3\ s^{-1}$); S_f is friction gradient and S_0 is channel slope. The equations were solved using the Newton–Raphson method (Stępień, 1984). The river-network parameters (e.g., flow direction, channel length, and channel slope) derived from a global river network database (Wu et al., 2012), and geomorphological parameters (e.g., channel width and channel depth) were obtained according to empirical hydraulic geometry relationships (Li et al., 2013, 2015) or remote sensing-based water surface extent data (Homer et al., 2015; Yamazaki et al., 2014).

2.4. In-Stream P Processes

The major in-stream P dynamics include decomposition and mineralization of organic matter, particle organic and inorganic matter deposition, P uptake and release by autotrophs, and adsorption and desorption between particle matter and dissolved P (Figure 1). Autotrophs assimilate DIP into cellular material, and form POP. DOP is eventually released or excreted by phytoplankton and is then further broken down to DIP through mineralization. DIP tends to attach to sediment particles and, thus, transforms to PIP. The net deposition of POP and PIP from water as sediment is a major P retention process in rivers. Riverine P dynamics were calculated within each grid-cell throughout both subnetwork flow and main channel flow. The dynamics of riverine P constituents are given by:

$$\frac{\Delta M_{POP}}{\Delta t} = F_{POP} + U_{DIP} - v_s\, A_s\, c_{POP} - R_{POP}\, M_{POP} \tag{10}$$

$$\frac{\Delta M_{DOP}}{\Delta t} = F_{DOP} + R_{POP}\, M_{POP} - R_{DOP}\, M_{DOP} \tag{11}$$

$$\frac{\Delta M_{DIP}}{\Delta t} = F_{DIP} + R_{DOP}\, M_{DOP} - U_{DIP} - A_{DIP} \tag{12}$$

$$\frac{\Delta M_{PIP}}{\Delta t} = F_{PIP} + A_{DIP} - v_s\, A_s\, c_{PIP} \tag{13}$$

where M_x is the total mass of constituent x (DIP, DOP, POP, PIP) in the main channel or subnetwork (g P); c_x is the concentration of x in water bodies ($mg\ L^{-1}$); Δt is the time step (hour); F_x is advective P transport from upstream or land (g P $hour^{-1}$) and the land P inputs are assumed to enter into streams at a constant rate within a day; U_{DIP} represents the uptake of phosphate by phytoplankton (g P $hour^{-1}$); v_s is the net deposition rate (m $hour^{-1}$); A_s is the surface area of the water body (m^2) obtained from the remote sensing products (Allen & Pavelsky, 2018; Homer et al., 2015); R_{POP} represents the desorption and excretion rate of particulate organic P ($hour^{-1}$); R_{DOP} is the mineralization rate coefficient of dissolved organic P ($hour^{-1}$); and A_{DIP} is the net adsorption of DIP (g P $hour^{-1}$) (negative value represents the desorption of PIP).

The deposition velocity of particulate matter is calculated according to Stokes' law (Thomann & Mueller, 1987):

$$v_s = 0.033634\, \alpha\, (\rho_s - \rho_w)\, d^2 \tag{14}$$

where ρ_s and ρ_w are the density of water and particulate matter ($g\ cm^{-3}$), respectively; α refers to the effect of the particle shape on the settling velocity (unitless) and d is the average diameter of the particulate matter (μm) (Chapra, 2008).

Table 1
Phosphorus Export-Related Parameters in the Dynamic Land Ecosystem Model-Terrestrial/Aquatic Scheme

Parameters	Unit	Values in DLEM	Description	References
b_{DIP}	Dimensionless	200–800	Adsorption capacity of soil for labile P	Calibrated
a	Dimensionless	11.8–20.2	Coefficient in the MUSLE	(Neitsch et al., 2011)
b	Dimensionless	0.56	Coefficient in the MUSLE	(Neitsch et al., 2011)
d	μm	1–10	Average diameter of the particulate matter	(Chapra, 2008)
Q_{10}	Dimensionless	2	Change fraction of the P reaction rate for a temperature change of 10°C;	(Kätterer et al., 1998)
k_{mDOP}	$hour^{-1}$	0.00008–0.0004	Base of mineralization rate of DOP	(Koehler et al., 2012)
k_{mPOP}	$hour^{-1}$	0.00002–0.0004	Base of excretion and desorption rates of POP	(Enríquez et al., 1993)
k_a	$m^3\ g^{-1}\ hour^{-1}$	0.416	Adsorption rate in water	(van der Zee et al., 1989)
k_d	$hour^{-1}$	0.15	Desorption rate in water	(van der Zee et al., 1989)

The excretion and mineralization rates of the organic P are consistent with the decomposition rate of organic matter, which can be estimated by a first-order kinetics equation with temperature dependence:

$$R_{DOP,POP} = k_{mDOP,mPOP}(Q_{10})^{\frac{T-T_s}{10}} \quad (15)$$

where $k_{mDOP,mPOP}$ is the base of excretion and mineralization rates of the organic P ($hour^{-1}$); Q_{10} is the change fraction of the P reaction rate for a temperature change of 10°C; T is the water temperature (°C) and T_s is the reference temperature (20°C).

The uptake of DIP by phytoplankton is linearly related to primary production in aquatic ecosystems, with C, N, and P coupling in this process. The uptake of DIP is estimated according to the method proposed in Maavara et al. (2015, 2017), which assumes the primary production is limited by P.

$$U_{DIP} = Pro \cdot RPC_{phyto} \quad (16)$$

$$Pro = Pro_{max} \cdot \frac{c_{DIP}}{K_s + c_{DIP}} \quad (17)$$

where Pro is primary production in aquatic ecosystems (g C $hour^{-1}$) and RPC_{phyto} is the P:C ratio of phytoplankton (set as 0.025 according to the Redfield ratio); K_s is the half-saturation DIP concentration (0.62–21.7 mg L^{-1}); Pro_{max} is the maximum value of primary production under nutrient saturated condition (g C $hour^{-1}$), which is calculated as:

$$Pro_{max} = B \cdot P_{chl} \cdot V \cdot M \quad (18)$$

where B is average depth-integrated chlorophyll concentration (mg Chl-a km^{-3}) which is calculated based the method provided by Reynolds (2006); P_{chl} is the maximum chlorophyll-specific carbon fixation rate (2.5 g C (mg Chl-a)$^{-1}$ hr^{-1}), V is water volume (km^3), and M is the metabolic correction factor for water temperature, which is equal to 1 when water temperature is higher than 28°C, and decreases with temperatures with a Q_{10} of 2 (Lewis Jr, 2011).

The adsorption-desorption process is estimated by using the kinetic form of the Langmuir sorption isotherm equation (McGechan & Lewis, 2002; van der Zee et al., 1989):

$$A_{DIP} = k_a \cdot c_{DIP} \cdot (A_{max} - M_{PIP}) - k_d \cdot M_{PIP} \quad (19)$$

where k_a is adsorption rate constant ($m^3\ g^{-1}\ hour^{-1}$) and k_d is and desorption rate constant ($hour^{-1}$), respectively; A_{max} is maximum P sorption capacity of particulate matter (g P). The major parameters introduced in this study were given in Table 1.

Table 2
Sensitivity of Riverine P Fluxes to Major Parameters in Dynamic Land Ecosystem Model

Parameters	Changes in parameters	Changes in DIP	Changes in DOP	Changes in POP	Changes in PIP	Changes in TP
b_{DIP}	10%	−7.33%	0.00%	0.00%	−0.01%	−1.99%
	−10%	8.96%	0.00%	0.00%	0.01%	2.43%
a	10%	0.09%	3.16%	10.72%	10.40%	7.16%
	−10%	−0.07%	−2.59%	−8.78%	−8.52%	−5.87%
d	10%	−0.02%	−0.23%	−0.98%	−1.23%	−0.82%
	−10%	0.02%	0.22%	0.90%	1.17%	0.78%
k_{mDOP}	10%	0.64%	−2.67%	0.00%	0.00%	0.00%
	−10%	−0.67%	2.79%	0.00%	0.00%	0.00%
k_{mPOP}	10%	0.14%	2.38%	−2.74%	0.00%	0.00%
	−10%	−0.14%	−2.47%	2.84%	0.00%	0.00%
k_d	10%	6.25%	0.00%	0.00%	−2.71%	0.07%
	−10%	−6.66%	0.00%	0.00%	2.89%	−0.08%

2.5. Parameter Sensitivity Analysis

Six key parameters controlling P fluxes were selected to conduct local sensitivity analyses based on our model calibration experience (Table 2). The riverine DIP export is most sensitive to the b_{DIP} and k_d, reflecting the important role of land leaching and adsorption-desorption processes within streams. The riverine DOP export shows similar responses (varied around 2%–3%) to a, k_{mDOP}, and k_{mPOP}. Changes in POP and PIP are predominantly controlled by the land erosion process (a). The TP export is generally more sensitive to land P inputs-related parameters (b_{DIP} and a) compared with in-steam retention-related parameters (d).

2.6. Data Sources

Several datasets were developed or collected to characterize natural and human forcing in the MRB (Table 3 and Table S1 in Supporting Information S1). Based on the datasets, all the required input data for the model

Table 3
Major Model Input Data and Validation Data

Data variables	Time period/step	Reference/source
Model input data/Environmental Drivers		
Climate (Temperature, Precipitation)	1901–2018/daily	GRIDMET (1979–2018) (http://www.climatologylab.org/gridmet.html) CRUNCEP (1901–1978) (https://doi.org/10.5065/PZ8F-F017)
Land Cover and Land Use (Crop density)	1901–2016/yearly	(Yu & Lu, 2018)
Atmospheric CO_2	1901–2018/yearly	NOAA's Earth System Research Laboratory (http://www.esrl.noaa.gov/gmd/ccgg/trends/) (Joos & Spahni, 2008)
P fertilizer application rate	1901–2018/yearly	USDA National Agricultural Statistics Service (https://quickstats.nass.usda.gov/)
Manure P production	1901–2017 yearly	(Bian et al., 2021)
P deposition rate	Annual average	(Mahowald et al., 2008)
Model Calibration and Validation data		
River discharge, Water quality (DIP, TDP, TP) in USGS sites: 07022000, 06934500,	1979–2018 daily	USGS National Water Information System (https://waterdata.usgs.gov/nwis)
P loads (DIP, TP) in USGS sites: 03612600, 07263620	1979–2018 monthly	USGS National Water Quality Network (https://nrtwq.usgs.gov/nwqn/#/)
P loads (DIP, TP) from the whole MRB to the Gulf of Mexico	1980–2018 annually	USGS National Water Quality Network (https://nrtwq.usgs.gov/nwqn/#/GULF)

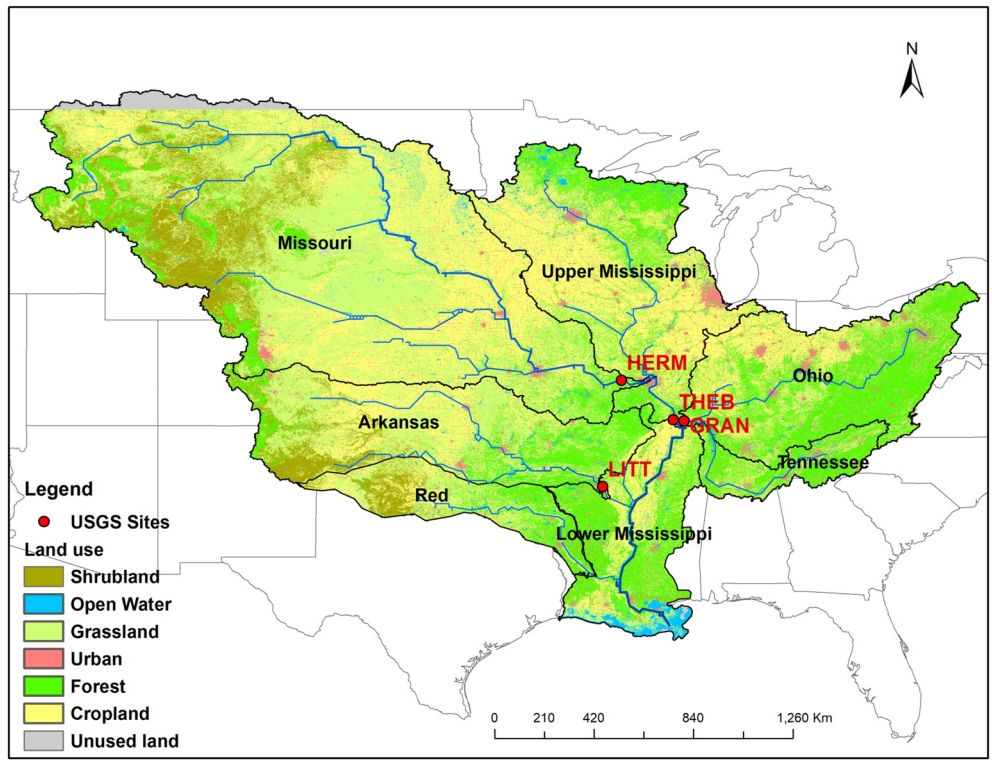

Figure 3. The Mississippi River Basin. USGS sites used for model calibration/validation include HERM (06934500), THEB (07022000), GRAN (03612600), LITT (07263620). Land use condition is derived from the National Land Cover Database 2016.

simulation (e.g., climate, land use, river network, soil properties, atmospheric CO_2, N inputs, P inputs, etc.) were developed at or resampled into a spatial resolution of 5 × 5 arc-min. The daily climate data from 1979 to 2018, including precipitation, temperature, etc., were obtained from GRIDMET (Abatzoglou, 2013), and climate data before 1979 were downscaled from the CRUNCEP data set (Viovy, 2018) and bias-corrected to GRIDMET. Atmospheric CO_2 data were derived from the Global Carbon Project, and were generated by merging ice core CO_2 data (Joos & Spahni, 2008) with National Oceanic and Atmospheric Administration (NOAA) annual resolution from 1958 onwards. P fertilizer application data were developed based on crop-specific application data from the USDA National Agricultural Statistics Service (https://quickstats.nass.usda.gov/) and combined with cropland distribution maps. Since USDA only provided P fertilizer data after 1960, we assumed the changing trend of P fertilizer in the U.S. during 1860–1960 was consistent with global agricultural P fertilizer usage (Cordell et al., 2009). More details regarding P fertilizer data development can be found in the supplementary material (Text S2 in Supporting Information S1). Manure P data were derived from the gridded manure P production and application data set in the U.S. developed by Bian et al. (2021). Both P fertilizer and manure application increased rapidly from the 1940s to the 1970s (Figure 2b). Yearly P deposition data were extracted from a global P deposition map (Mahowald et al., 2008). P deposition only accounted for a small share (around 1% in 2000) of the TP input to terrestrial ecosystems compared to other sources. For LUC, cropland expanded rapidly from 1901 to 1930 but decreased dramatically during 1955–1965 due to cropland abandonment; thereafter, cropland area increased again and stayed relatively stable after the 1980s (Figure 2c).

The MRB, draining 4.76 million km^2, encompasses 41% of the contiguous U.S. and is the largest contributor of fresh water and nutrients to the Gulf of Mexico. The MRB consists of seven major sub-basins, including Upper Mississippi, Ohio, Missouri, Arkansas, Red, Tennessee, and Lower Mississippi River basins (Figure 3). River discharge and water quality data of four USGS sites in the MRB at the outlet of major sub-basins were selected to calibrate and validate the DLEM–Terrestrial/Aquatic scheme simulated results. Near the outlet of the Lower MRB, around 30% of the flow is diverted down the Atchafalaya River through the Old River Control Structure. The riverine transport in DLEM was simulated based on the river network and flow direction data derived from

topographic data (Wu et al., 2012) and cannot capture this human-controlled flow diversion. Instead of validating P fluxes at USGS sites inside the Lower MRB, we validated the riverine P export from the whole basin by comparing the simulated P exports from the MRB with the annual P exports data reported by USGS (https://nrtwq.usgs.gov/nwqn/#/GULF), which combined the observed loading data from sites on both the Mississippi River and Atchafalaya River (Lee et al., 2017).

To obtain continuous monthly P flux data based on water quality data from the four USGS sites, the Weighted Regressions on Time, Discharge, and Season (WRTDS) method was applied to calculate monthly DIP, total dissolved P (TDP), and TP loading from 1979 to 2018 (Hirsch et al., 2010). However, the WRTDS method cannot be directly applied at two sites (USGS 03612600 in Ohio/Tennessee, 07263620 in Arkansas) where long-term daily discharge data were not available from the USGS National Water Information System. So, we acquired the long-term monthly P loading data (DIP and TP) at these three sites from the USGS National Water Quality Network where monthly P loading in MRB has been assessed. The model outputs have four P components (DIP, DOP, POP, and PIP), but only three major P variables (DIP, TDP, and TP) can be provided by the USGS for validation. TDP (only available at USGS 06934500 in Missouri and 07022000 in Upper Mississippi) is the sum of DOP and DIP, and the difference between TP and TDP is particulate form P (PP), including POP and PIP. Simulated DOP can be indirectly validated according to the accuracy of simulated DIP and TDP; similarly, simulated PP can be validated by combining TP and TDP. However, the USGS data cannot support the validation of POP and PIP separately. To address this issue, we assumed the riverine POP had a stable ratio relationship with particulate organic carbon (POC). By verifying simulated riverine POC and PP, the simulated POP and PIP were validated indirectly (Yao et al., 2021). The USGS data before 2000 were used for model calibration and the data after 2000 were used for model validation.

2.7. Simulation Experiments

The DLEM–Terrestrial/Aquatic scheme simulations included three steps: (a) an equilibrium run that used 40-year (1861–1900) mean climate datasets to develop the initial state under the pre-1900 conditions; (b) a spin-up simulation that was performed to eliminate noise caused by the simulation shift from the equilibrium to the transient simulation; (c) a transient simulation using 118 years (1901–2018) of forcings to generate results. Six simulation experiments (S0-S5), following a "without" strategy, were designed to study natural and anthropogenic impacts on riverine P loading (Table S2 in Supporting Information S1). All the simulations started from the same baseline equilibrium state. S0 (All combined) is the reference simulation with all the dynamic forcings. In experiment S1, the climate variables were fixed as the annual averages of climate data from 1901 to 1920. In experiments S2–S5, one of the forcings (CO_2, P fertilizer, P manure, and Land-use) was fixed in 1901, while other forcings varied with time. The differences between S1–S5 and S0 were taken as the impacts of the corresponding factors.

3. Results

3.1. Model Performance

The coefficient of determination (R^2) and Nash–Sutcliffe efficiency (*NSE*) were used to compare the simulated monthly results and USGS observed data. Target diagrams (Jolliff et al., 2009) provide information regarding the bias and Root–Mean–Square Difference (*RMSD*) of the simulated results (Table 4 and Figure 4). Generally, the model could catch the variations and magnitudes of riverine DIP, TDP, and TP fluxes in the major sub-basins of MRB. For riverine DIP flux, the R^2 values ranged from 0.33 to 0.63, and *NSE* ranged from 0.32 to 0.59. The target diagram shows that the simulated results slightly overestimated DIP flux in the Ohio River, but slightly underestimated DIP flux in the Upper Mississippi River. The temporal variation of DIP fluxes agreed well with USGS data in most rivers except the Arkansas, where simulated DIP underestimated the peaks (Figure S4). For riverine TDP flux, the model performed well in the Missouri and Upper Mississippi Rivers, with low biases (Figure 4) and R^2 values ranging from 0.43 to 0.61 and *NSE* ranging from 0.23 to 0.57. The simulated riverine TP flux was overestimated in the Arkansas River but had very slight biases for other rivers, with R^2 values ranging from 0.26 to 0.70, and *NSE* ranging from 0.21 to 0.65. It was noted that the simulated results underestimate the numerous peaks of TP fluxes in the Missouri and Upper Mississippi Rivers. The model performed better in the validation period than the calibration period for Missouri and Arkansas Rivers, and the opposite was seen for the Ohio River.

Table 4
Evaluation of Simulated Results Against Field Data

Sub-basins (USGS sites)		TDP		DIP		TP	
		R^2	NSE	R^2	NSE	R^2	NSE
Missouri (HERM)	Calibration	0.43	0.23	0.46	0.37	0.26	0.21
	Validation	0.58	0.55	0.58	0.53	0.35	0.28
Upper Mississippi (THEB)	Calibration	0.57	0.57	0.59	0.57	0.47	0.46
	Validation	0.61	0.56	0.61	0.53	0.50	0.46
Ohio/Tennessee (GRAN)	Calibration			0.63	0.59	0.60	0.59
	Validation			0.50	0.47	0.54	0.51
Arkansas (LITT)	Calibration			0.33	0.32	0.53	0.42
	Validation			0.49	0.44	0.70	0.65

Note. The temporal DLEM-simulated flow and P load results against USGS data can be found in supplementary (Figures S3 and S4 in Supporting Information S1).

The average simulated DIP and TP exports from the MRB matched well with USGS observed data, though the interannual variation of P fluxes still showed discrepancies (Figure 5). The slope of simulated DIP export (0.14 Gg P yr^{-2}, $p = 0.20$) during 1980–2018 was similar to that of observed DIP export (0.15 Gg P yr^{-2}, $p = 0.39$), although the increasing trends were not significant ($p > 0.05$). The simulated TP export increased at a rate of 1.03 Gg P yr^{-2} ($p = 0.02$) during 1980–2018, which was higher than the rate of observed TP export (slope = 0.77 Gg P yr^{-2}, $p = 0.07$). The simulated TP export slightly overestimated the increasing trend of TP export in recent decades.

3.2. Temporal Pattern of P Fluxes During 1901–2018

The simulated DIP, DOP, POP, and PIP exports from the MRB all exhibited obvious inter-annual fluctuations (Figure 6). Simulated riverine DIP export increased by 42%, from 36.3 Gg P yr^{-1} in the 1900s (1901–1909) to 51.6 Gg P yr^{-1} in the post-2010s (2010–2018). The fastest growth of simulated DIP occurred during 1963–1973, at a rate of 2.0 Gg P yr^{-2}. After the 1970s, simulated DIP fluctuated around a stable value. Simulated riverine DOP export experienced a drop around the 1950s and 1960s, then increased in the 1970s, and leveled off thereafter, reaching 10.8 Gg P yr^{-1} in the post-2010s. Simulated POP and PIP exports, which exhibited a similar interannual variation pattern, increased by 59% (from 10.8 to 17.1 Gg P yr^{-1}) and by 54% (from 62.0 to 95.2 Gg P yr^{-1}), respectively, from the 1900s to the post-2010s. The growth rate of simulated POP and PIP had accelerated after the 1960s, at rates of 0.5 Gg P yr^{-2} and 0.1 Gg P yr^{-2}, respectively, during 1960–2018. The peak values of simulated P exports also became higher in some years of recent decades (e.g., 1993 and 2018). The PIP flux dominated

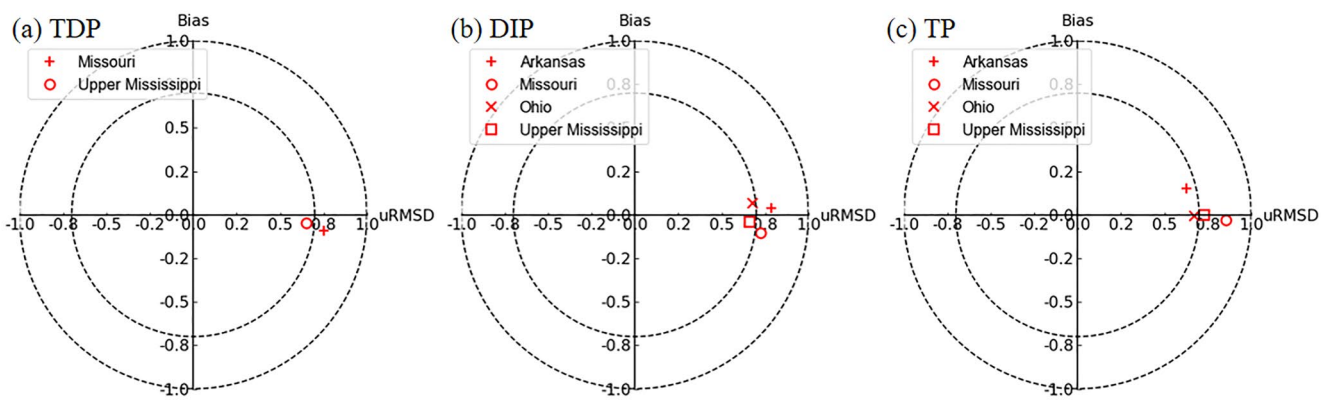

Figure 4. Normalized target diagrams for monthly (a) TDP, (b) dissolved inorganic phosphorus, and (c) TP comparisons between simulations and USGS data (1979–2018). (The *X*-axis is unbiased total Root–Mean–Square Difference (uRMSD), and *Y*-axis is normalized bias. Both axes are normalized by the standard deviation of USGS data).

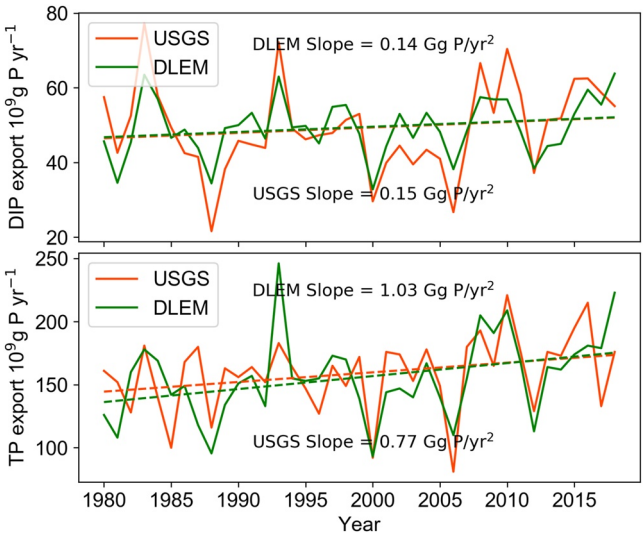

Figure 5. The comparison of USGS-observed and DLEM-simulated annual riverine dissolved inorganic phosphorus and TP exports from the Mississippi River Basin during 1980–2018.

the P export, accounting for 48%–54% of TP export, followed by DIP flux, accounting for 30%–35% (Figure S5 in Supporting Information S1). The POP and DOP fluxes contributed 6%–8% and 9%–10% to TP flux, respectively. The decadal average of TP export increased significantly since the 1960s and reached 163.1 Gg P yr^{-1} in the 1990s, then declined in the 2000s, but increased again to 174.8 Gg P yr^{-1} in the 2010s. From the 1960s to the post-2010s, DIP, DOP, POP, PIP, and TP increased by 42%, 53%, 60%, 53%, and 50%, respectively.

3.3. Spatial Variability of P Yields

Yields of different P species showed different distribution characteristics which became noticeable especially after 1980 (Figure S6 in Supporting Information S1). Simulated DIP yield decreased along a gradient from the central part (mainly cropland) of the MRB to both sides. DOP yield was high in the central and eastern basin where forest and cropland dominated, and low in the western part which was mainly covered by grassland and shrubland. With respect to change rates after 1980, DIP yield increased mostly in the cropland area (western Ohio, Upper Mississippi, and eastern Missouri) (Figures 3 and 7a). By contrast, DOP yield increased in almost the entire Ohio and slightly decreased in central Upper Mississippi and southern Lower Mississippi (Figure 7c). The distribution of simulated PIP and POP yields were similar, with high-yield regions concentrating on several hot spots (e.g. eastern Ohio, Upper Mississippi, western Missouri) (Figure S4 in Supporting Information S1). However, the change rates of PIP and POP yields were distributed more evenly (Figures 7b and 7d), with an increasing trend across most of the MRB except western Missouri. Compared to the other three P species, the change rate of DIP yield showed large spatial variability. It showed the fastest increase (>0.0006 g P m^{-2} yr^{-2}, $p < 0.05$) in some regions like western Ohio and Upper Mississippi but the most rapid decrease (<–0.0004 g P m^{-2} yr^{-2}, $p < 0.05$) in southeastern of Missouri, southern Lower Mississippi, and eastern Tennessee.

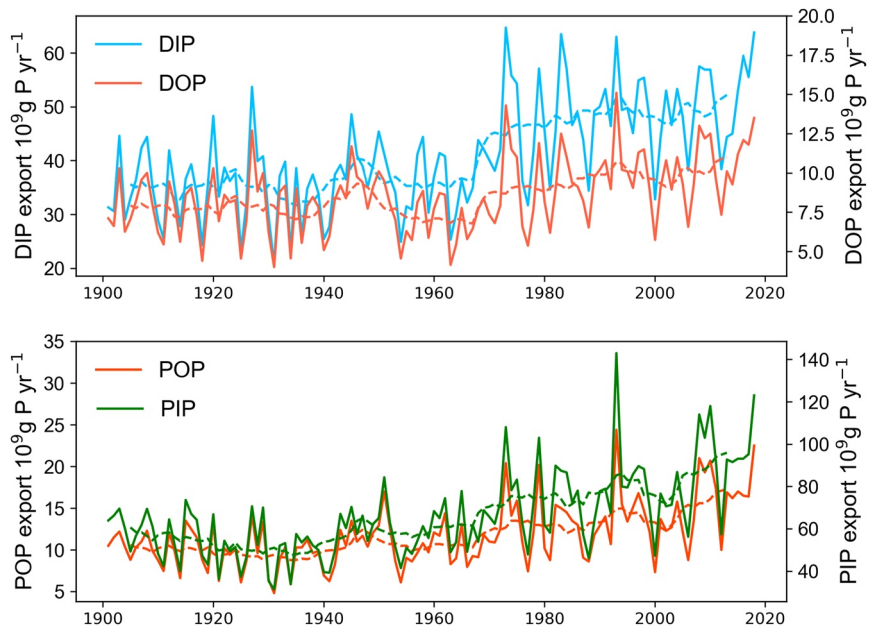

Figure 6. Interannual variation and trend in simulated dissolved inorganic phosphorus, dissolved organic phosphorus, particulate organic phosphorus, and particulate inorganic phosphorus fluxes from the Mississippi River Basin during 1901–2018. Dash lines are 10-year moving averages of P fluxes (The value in year i is the average P export from year $i-4$ to $i+5$).

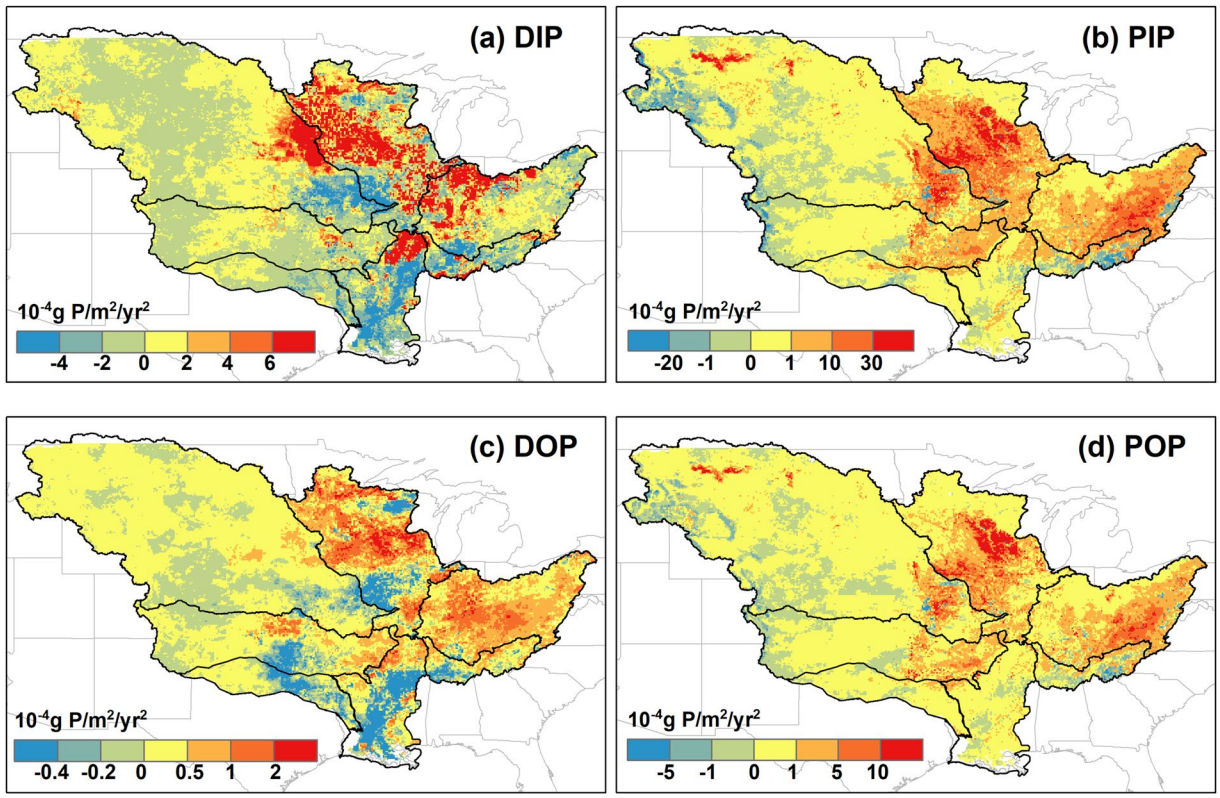

Figure 7. Annual change rates (1980–2018) in P yields: (a) Dissolved inorganic phosphorus, (b) particulate inorganic phosphorus, (c) dissolved organic phosphorus, and (d) particulate organic phosphorus.

3.4. Contributions of Multiple Environmental Factors to Changes in P Loading

The increasing trends of different P components were dominated by different environmental factors (climate, fertilizer, manure, atmospheric CO_2, and land use), and the same factor might have opposite impacts on different P components (Figure 8). Riverine DIP loading is dominated by the increasing application of P fertilizer and manure after the 1950s. The simulated DIP export from 2010–2018 in S0 (reference simulation) is 27% higher than S3 ("constant fertilizer" simulation), and 17% higher than S4 ("constant manure" simulation). The LUC, especially cropland expansion, is the second important contributor to DIP export. Compared to S5 ("constant LUC" simulation), DIP export in S0 was 33% higher in the 1980s and 26% higher during 2010–2018. Climate variability and P fertilizer are two primary contributors to PIP export since the 1970s. Averaged over 2010–2018, the simulated export of PIP in S0 was higher than that in S1 ("constant climate" simulation) by 32% and S3 by 23%. LUC decreased the PIP export through the study period, and its impact was more pronounced before the 1940s as cropland expanded but weakened thereafter when cropland abandonment occurred. The changes in DOP and POP exports were dominated by two major factors, climate and LUC. The contributions of climate to DOP and POP exports magnified in recent decades, and during 2010–2018, the exports of simulated riverine DOP and POP in S0 increased by 31% and 43%, respectively, compared with S1. LUC decreased DOP and POP exports by around 3% and 16% over 2010–2018, respectively. Since the 1970s, the rising atmospheric CO_2 concentration gradually increased the DOP export and played an increasingly important role in decreasing DIP and PIP exports.

In summary, climate (precipitation and temperature) variability and P fertilizer usage were the two key factors that increased TP loading since the 1970s (Table 5). The impacts of fertilizer application and animal manure on TP export continually increased throughout the study period, and climate induced the highest TP export (37.50 Gg P yr^{-1}) after 2010. Atmospheric CO_2 was the only factor that declined TP export since 1901, decreasing around 14.35 Gg P yr^{-1} export during 2010–2018. LUC first decreased TP export until the 1970s, and then started to increase TP export thereafter.

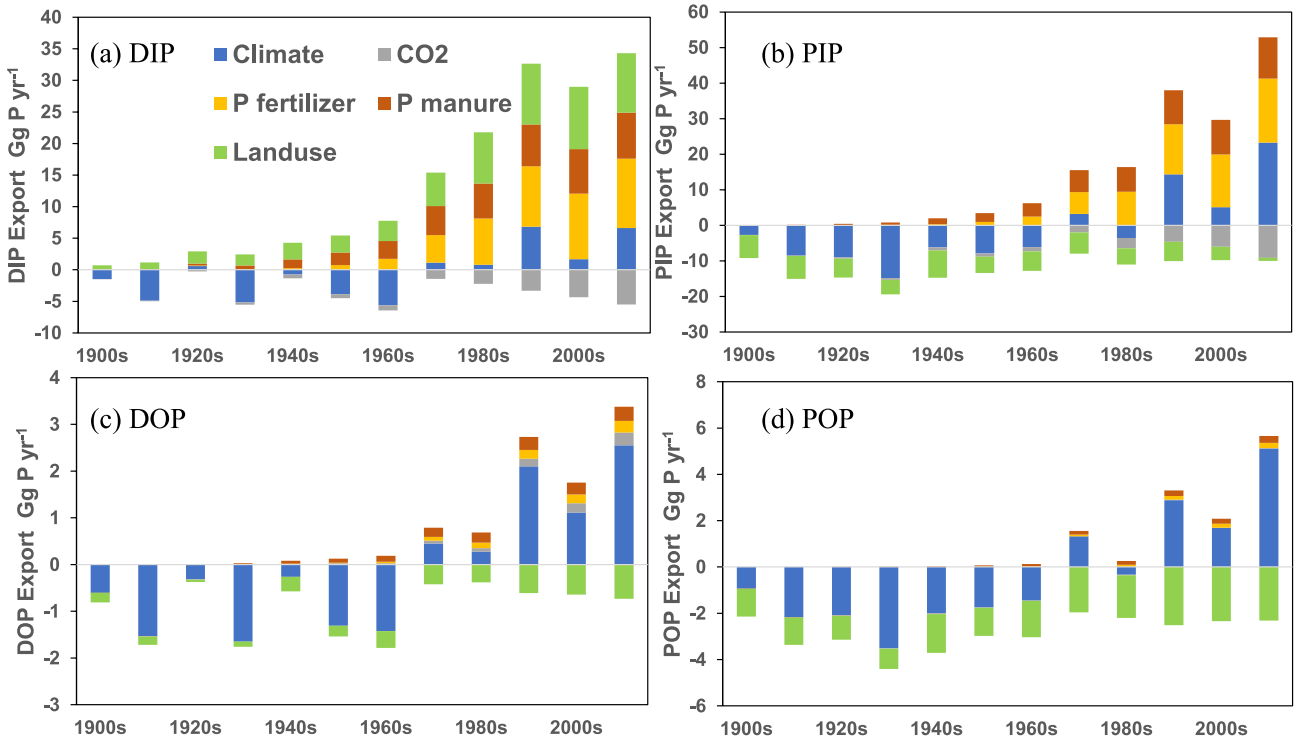

Figure 8. Decadal changes in the contributions of environmental factors on riverine (a) dissolved inorganic phosphorus, (b) particulate inorganic phosphorus, (c) dissolved organic phosphorus, and (d) particulate organic phosphorus exports. Contributions were the cumulative difference between the reference simulation (S0) and counterfactual scenario (S1–S5) (see Section 2.7 and Table S2 in Supporting Information S1).

4. Discussion

4.1. Importance of Integrating Terrestrial and Aquatic Processes

The delivery of P from land to ocean through river systems is the major pathway for P leaving terrestrial and entering coastal ecosystems. Studies on P loading across the land-ocean interface call for a connection of P fluxes between terrestrial and aquatic ecosystems. However, due to the physical and biological differences between aquatic and terrestrial ecosystems, the modeling approaches for terrestrial and aquatic biogeochemistry have developed somewhat independently (Bouwman, Bierkens, et al., 2013; Bouwman, Goldewijk, et al., 2013). Our study fills a critical gap by integrating a terrestrial biogeochemical model with an aquatic biogeochemical module and connecting the cycle of different P species between terrestrial and aquatic ecosystems. The DLEM–Terrestrial/Aquatic scheme is capable of simulating P fluxes across parent material, soil, and vegetation to headwaters, main-channel rivers, and eventually river outlets. The full consideration of terrestrial and aquatic processes in the DLEM–Terrestrial/Aquatic scheme can provide both prognostic and predictive assessments of interactions of P dynamics among soil, water, and vegetation. Furthermore, impacts of human disturbances on P loading can be tracked under multiple environmental conditions. Independent aquatic models usually rely on detailed boundary conditions and are applied at relatively short-time scales (hour, day, month, year), while terrestrial biosphere models can be applied over long-time scales (decade, century). With terrestrial modules providing long time scale P input for aquatic modules, the DLEM–Terrestrial/Aquatic scheme can be used to investigate P loading at time scales from days to century. Simultaneously, the scale-adaptive water and nutrient transport scheme can simulate the delivery

Table 5
Decadal Changes in the Differences of Riverine TP Export Between the Reference Simulation (S0) and Scenario Simulations (S1–S5)

Year	Climate	CO_2	P Fertilizer	P Manure	LUC
1900s	−5.74	−0.05	0.00	0.02	−7.17
1910s	−17.13	−0.24	0.05	0.17	−6.71
1920s	−10.86	−0.63	0.16	0.66	−4.40
1930s	−25.20	−0.85	0.24	1.25	−3.31
1940s	−9.25	−1.46	0.59	3.11	−7.06
1950s	−14.81	−1.56	1.73	4.59	−3.36
1960s	−14.61	−2.04	4.25	6.80	−4.20
1970s	6.10	−3.40	10.69	11.14	−3.03
1980s	−2.80	−5.10	16.99	12.85	1.32
1990s	26.16	−7.79	23.95	16.78	1.06
2000s	9.56	−10.17	25.61	17.28	3.12
2010s	37.50	−14.35	29.51	19.47	5.52

Note. Unit: Gg P yr^{-1}.

process at the sub-grid level by incorporating hillslope flow, subnetwork flow, and main-channel flow. Thus, our model is capable of simulating P transport at multiple spatial scales from basin to continental to global (Yao et al., 2020).

Another important advantage of the DLEM–Terrestrial/Aquatic scheme is having the ability to estimate the export of four riverine P species: DIP, DOP, PIP, and POP. DIP, as reactive P, is available for biological uptake and links the P and C cycles (Compton et al., 2000). DIP in fresh waters and coastal waters directly impacts the primary productivity of aquatic ecosystems and excessive DIP leads to eutrophication. The riverine DIP concentration is not only shaped by its abundance in local rocks and soils, but also by physical and biochemical transformations between different P species. In the soil environment, P ions are easily adsorbed to particles and colloids and co-precipitate with chemicals such as iron and calcium. As P enters the river in particulate form, P ions could be released and become bio-available if changes in iron/aluminum/calcium concentrations, temperature, pH, and redox conditions favor desorption process (Bai et al., 2017). Generally, DIP can be regarded as an immediately available nutrient source to aquatic biota, while particulate form P represents a longer-term source (McDowell et al., 2004). Meanwhile, the settling of PP is a major P detention process and riverine PP has the largest share in TP, thus the removal of P in water column may be enhanced if settling process is favored. The turnover rate of P between organic and inorganic forms is closely related to primary productivity and varies both spatially and seasonally (Heidel et al., 2006). Therefore, the concentrations and distributions of different P species in aquatic systems can change rapidly due to both biogeochemical cycling processes and local P loading. Additionally, in consideration of the behavior of different forms of P in aquatic systems, the assessment of riverine export of multiple P species can provide detailed information for the further study of coastal ocean ecosystem processes.

4.2. Climate and Anthropogenic Control Over P Loading

In this study, the simulation experiments provided an evaluation of the individual contributions of multiple environmental factors to riverine P exports and offered insight into the mechanisms behind the responses. The major reasons for the increases of different P species in the MRB varied. Riverine DIP export was mainly driven by the increased usage of fertilizer while PIP, DOP, and POP exports were primarily driven by increased precipitation. The joint effect of climate and anthropogenic activities shaped temporal and spatial patterns of P loading.

4.2.1. Climate Control Over P Loading

The magnitude and variation of P losses from land are directly influenced by climate, especially precipitation (Jennings et al., 2009). Climate impacts the reaction rates of biogeochemical transformations, such as weathering, decomposition, mineralization, and plant uptake. Climate also regulates the hydrological processes that modify the yield and transport of P across terrestrial and aquatic systems. The inter-annual variations of riverine DIP, PIP, DOP, and POP exports were strongly influenced by inter-annual variations in precipitation (Figures 3a and 6). The peaks of P exports consistently occurred in wet years (e.g., 1993 and 2008), while the lowest P exports occurred in dry years (e.g., 2000, 2006, and 2012). At the decadal scale, the 1950s drought was associated with low P exports, while rising precipitation and warming enhanced the exports of TP in recent decades (Figure 8). The intensified weathering under the condition of wetting and warming facilitated the transformation of P from mineral to biologically available form (Goll et al., 2014). The increasing P involved in the mobilization associated with the rising runoff contributed to the increasing trends of P exports. With regard to spatial patterns of P loading, conditions of relatively high precipitation contributed to high P yields in the central and eastern portion of the basin, especially for DOP yield (Figure S4 in Supporting Information S1). High precipitation stimulated plant growth and ecosystem productivity, which could then further promote the accumulation of soil organic matter and modify the allocation of P in soil. High rates of leaching and organic P storage contributed to the high DOP yield in the eastern basin. Except agricultural areas, climate-related factors dominated the change in P loading in most regions.

4.2.2. Anthropogenic Control Over P Loading

In most agricultural soils, weathering results in slow release of P that is readily absorbed by crops or combined with aluminum, iron, calcium, and manganese, whereas application of mineral fertilizer can temporarily enhance the dissolved form of P. According to McDowell et al. (2004), application of P increased DIP that was subsequently lost to overland flow at levels 4–26 times greater than that of unamended soil. Meanwhile, around 28% of P may remain in agricultural soil and become legacy P (Kleinman et al., 2011; MacDonald et al., 2012).

For DLEM–Terrestrial/Aquatic scheme, the legacy P in agricultural soil was from the accumulated labile P, secondary mineral P, and occluded P pools after fertilizer application (Figure 1). The soil legacy P, which can be a continuous source of soluble and particulate P released into waters, has raised concern in recent years (Rowe et al., 2016; Sabo et al., 2021). In this study, the consumption of P fertilizer was relatively stable after the 1980s (Figure 2b), but the contribution of fertilizer to TP loading continued to increase into the 2010s (Table 5). The soil legacy P has been shown to weaken the efficacy of conservation measures across watersheds and thus more effective nutrient management strategies may be required (Sharpley et al., 2013). Additionally, the P use efficiency (PUE) of crops has increased in some regions of the MRB as crop yields continued increasing while P fertilizer application keep relatively stable during the post-1980 period (Swaney & Howarth, 2019). The improved PUE in crop production could reduce the DIP yield in several agricultural areas (Figure 7).

Land-use change influences P loading by modifying the allocation of P inputs to soil and the resistance of soil to erosion. Croplands receives most mineral P fertilizer and are vulnerable to soil erosion, while harvested crops transfer P out of the agricultural systems. With regard to other land cover types, such as forest, the majority of P circulates inside the vegetation–microbe–soil system (Sohrt et al., 2017). Before the wide use of mineral P fertilizers (around the 1940s), the expansion of cropland consumed the P storage in soil and decreased P loading. According to Tiessen et al. (1992), soil organic P storage can drop significantly in response to long-term cultivation and crop removal. After the 1940s, the application of mineral P fertilizer increased quickly and the P losses from cropland were intensified. By contrast, extensive cropland abandonment (Figure 2c) may, to some extent, alleviate P loss (Yu & Lu, 2018). Therefore, the impact of LUC on P loading varied with different types of land-use conversion and changed in different periods.

Elevated atmospheric CO_2 stimulates the plant growth and uptake of inorganic P (Terrer et al., 2019). Increased ecosystem primary production and C accumulation enhanced P immobilization into plant biomass and soil organic pools. As a result, inorganic P exports decreased while organic P exports increased in response to elevated atmospheric CO_2. As CO_2 emission continues rising, changing C cycle can potentially exert more influence on P cycle in terrestrial ecosystems and ultimately alter P export.

4.2.3. Interactive Effect of Climate and Anthropogenic Factors on Soil Erosion and P Loss

As the major portion of soil P is tightly adsorbed to mineral particles, bound within organic matter or precipitated as weakly soluble salts, soil erosion is the most crucial factor driving potential P loss from ecosystems (Alewell et al., 2020; Carpenter & Bennett, 2011). Soil erosion is influenced by many factors (including rainfall, land use condition, soil type, topography, and management), and large amounts of soil loss can happen rapidly (Quinton et al., 2010). PP loss does not occur from the entire catchment but rather from many critical source areas where serious soil erosion occurs or soil P content is high (McDowell et al., 2004). From a temporal perspective, the increased precipitation in recent decades in the MRB would have accelerated soil erosion and PP loss (Lu et al., 2020; Tan et al., 2021). Furthermore, in extreme precipitation events, higher rainfall intensity can exacerbate soil erosion and potentially cause huge soil P loss on short time scales (Carpenter et al., 2018; Z. Li & Fang, 2016). Anthropogenic management activities (e.g., overgrazing, intensive agriculture, and tile drainage) combined with related LUC are another primary cause of gradual change in soil erosion (Borrelli et al., 2017; Turner & Rabalais, 2003). Historically, erosion increased when forest cover was converted to cropland and declined when farms were abandoned (Turner & Rabalais, 2003). Cropland received most of the P inputs but also was vulnerable to erosion. Soil erosion accompanied by P loss has been recognized as a threat to soil P storage and food security, especially in places with low or no P fertilizer inputs (Bouwman, Goldewijk, et al., 2013; MacDonald et al., 2011). Due to the strong interaction between climate and anthropogenic factors, land management options for erosion control and soil P retention need to consider climate change adaptation.

4.3. Uncertainty and Limitation

In this study, the simulated results with DLEM–Terrestrial/Aquatic scheme can generally depict the magnitude and variation of P loading from the MRB on long-time scales. However, uncertainties remain due to limitations in the model structure and input datasets. The major component in riverine TP is the particulate form of P, which is derived from erosion and gradual settling during river transport process. Landscape soil erosion through overland flow is estimated in the model, but bank erosion and other geological hazards, like mass wasting, were not considered in this study. It is understood that historical soil erosion has left significant sediments within river valleys

and floodplains that are an important source for modern sediment in the MRB (Hassan et al., 2017). However, our simulated results may underestimate the sediment and PIP yields from river valleys in the Lower Mississippi.

From a temporal perspective, the peak values of P loading in Missouri and Upper Mississippi were underestimated in our simulations and may result from the underestimation of peak flows and the lack of accounting for resuspension processes in river channels. Extreme precipitation events and peak flow can potentially cause a higher magnitude of erosion. In this study, we assumed each grid represents a hydrological unit, and the peak flow calculated in grid cells may be underestimated compared to estimates for actual catchments. We also did not account for the interaction between bottom sediment and water column due to the unsound representation of biogeochemical processes inside river sediment in the current model. Some of the P in sediments in stream bottom can be introduced to the water column through resuspension (particulate form) or by diffusion (dissolved inorganic forms) (Vilmin et al., 2015). Resuspension can be significant when flow rate is high (Pulley et al., 2016). Therefore, the omission of resuspended P as source in our model leads to an underestimation of riverine P exports in the simulation, especially during peak flow.

Additionally, PP is more likely to be sequestered in dam reservoirs as the abundance of dams in the MRB may have enhanced the retention of P loads (Maavara et al., 2015). Sediment loads transported down the Lower Mississippi were reported to fall by more than half over the last century due to the trapping characteristic of dam and reservoir construction and in-channel storage (T. Li et al., 2020; Meade & Moody, 2010; Remo et al., 2017), and PP loads may experience a similar decline process. Considering the DLEM results were validated against observed data only in the recent decades, the simulated results may underestimate the P loading before the 1950s when reservoirs initially started to play a key role in reducing riverine sediment.

Moreover, the lock-and-dam systems construction, channel straightening, bank stabilization, the loss of wetlands, and occlusion of floodplain swamps in the basin during the twentieth century would affect P delivery to the Gulf but were not considered in this study. The neglecting of these physical changes may limit the efficacy of in-stream processes and introduce considerable uncertainty in the estimate of long-term P loading, especially during the early to middle part of the twentieth century. In the future, we plan to develop a process-based dam module within DLEM–Terrestrial/Aquatic scheme and build a more robust hydrological module to estimate the impact of dam and reservoir on nutrient loading.

The century-scale simulation is heavily dependent on a sizeable number of input datasets. Many assumptions were made to extend the datasets back to the preindustrial period. For example, P fertilizer data in the U.S. are only available after 1960, and the data before 1960 were estimated according to the global change trend of P fertilizer consumption, which brought uncertainties to the simulated P exports before 1960. Furthermore, several input datasets, such as P deposition and lithology data, were extracted from global datasets at 0.5°-arc resolution, and these were resampled to arc 5-min resolution to match other input data, potentially introducing spatial biases. Due to the unavailability of the dynamic and spatially explicit P point sources data in the MRB, we estimated P emissions from wastewater by applying an empirical method based on population and GDP. However, variations in wastewater P, especially those associated with reductions due to policy and technological changes, were hard to accurately estimate without specific data. Additionally, the annual P inputs, such as fertilizer and manure, were allocated on each day equally within the crop growing seasons, which ignored the impact of fertilizer and manure application timing on P dynamics at daily or seasonal scale.

5. Conclusions

This study developed a riverine P module coupled with a terrestrial biogeochemical model, the DLEM–Terrestrial/Aquatic scheme, to simulate P dynamics across the land–ocean aquatic continuum. The model linked P cycles in terrestrial and aquatic ecosystems and simulated the long-term dynamics of the loading and exports of four P species: DIP, DOP, PIP, and POP. The model was applied in the MRB and performed relatively well to simulate the magnitudes and variations of riverine P exports. The simulated results suggest that riverine PIP dominated the TP flux, while DOP had the smallest contribution. The estimated riverine DIP, DOP, PIP, and POP exports all increased over 1901–2018, but DIP and DOP exports leveled off after the 1970s. The increase in DIP export was mainly driven by elevated usage of P fertilizer and manure and increases in the other three P species were driven by increasing precipitation. The intense soil erosion accompanied by PP loss during extreme precipitation events appears to dominate the TP flux. LUC contributed to the increase of DIP load, but reduced

loads of DOP, POP, and PIP. Rising atmospheric CO_2 concentrations played an increasingly important role in decreasing DIP and PIP exports. This study highlights the impacts of changes in terrestrial ecosystems on P loading to aquatic systems, which is critical for sustainable nutrient management and water security in a changing global environment.

Data Availability Statement

The model-simulated annual land P yield maps and riverine P exports from the MRB are archived in the Box Cloud (https://auburn.box.com/s/30nnuw3d2f0ks5syzn7vfkin7cdyfoun). The model source code, input data, and row outputs in this study are accessible upon request (contact: tianhan@auburn.edu).

Acknowledgments
This study has been supported partially by NSF Grant (1903722; 1922687); NOAA Grant (NA16NOS4780204), and the NASA grants (NNX12AP84G, NNX14AO73G, NNX10AU06G). We thank three anonymous reviewers for their constructive comments that are very helpful for improving this paper.

References

Abatzoglou, J. T. (2013). Development of gridded surface meteorological data for ecological applications and modelling. *International Journal of Climatology*, *33*(1), 121–131. https://doi.org/10.1002/joc.3413

Aissa-Grouz, N., Garnier, J., & Billen, G. (2018). Long trend reduction of phosphorus wastewater loading in the seine: Determination of phosphorus speciation and sorption for modeling algal growth. *Environmental Science and Pollution Research*, *25*(24), 23515–23528. https://doi.org/10.1007/s11356-016-7555-7

Alewell, C., Ringeval, B., Ballabio, C., Robinson, D. A., Panagos, P., & Borrelli, P. (2020). Global phosphorus shortage will be aggravated by soil erosion. *Nature Communications*, *11*(1), 4546. https://doi.org/10.1038/s41467-020-18326-7

Alexander, R. B., Smith, R. A., Schwarz, G. E., Boyer, E. W., Nolan, J. V., & Brakebill, J. W. (2008). Differences in phosphorus and nitrogen delivery to the Gulf of Mexico from the Mississippi River basin. *Environmental Science & Technology*, *42*(3), 822–830. https://doi.org/10.1021/es0716103

Allen, G. H., & Pavelsky, T. M. (2018). Global extent of rivers and streams. *Science*, *361*(6402), 585–588. https://doi.org/10.1126/science.aat0636

Amundson, R., Berhe, A. A., Hopmans, J. W., Olson, C., Sztein, A. E., & Sparks, D. L. (2015). Soil and human security in the 21st century. *Science*, *348*(6235), 1261071. https://doi.org/10.1126/science.1261071

Bai, J., Ye, X., Jia, J., Zhang, G., Zhao, Q., Cui, B., & Liu, X. (2017). Phosphorus sorption-desorption and effects of temperature, pH and salinity on phosphorus sorption in marsh soils from coastal wetlands with different flooding conditions. *Chemosphere*, *188*, 677–688. https://doi.org/10.1016/j.chemosphere.2017.08.117

Bennett, E. M., Carpenter, S. R., & Caraco, N. F. (2001). Human impact on erodable phosphorus and eutrophication: A global perspective. *BioScience*, *51*(3), 227. https://doi.org/10.1641/0006-3568(2001)051[0227:HIOEPA]2.0.CO;2

Beusen, A. H. W., Van Beek, L. P. H., Bouwman, A. F., Mogollón, J. M., & Middelburg, J. J. (2015). Coupling global models for hydrology and nutrient loading to simulate nitrogen and phosphorus retention in surface water – Description of IMAGE–GNM and analysis of performance. *Geoscientific Model Development*, *8*(12), 4045–4067. https://doi.org/10.5194/gmd-8-4045-2015

Bian, Z., Tian, H., Yang, Q., Xu, R., Pan, S., & Zhang, B. (2021). Production and application of manure nitrogen and phosphorus in the United States since 1860. *Earth System Science Data*, *13*(2), 515–527. https://doi.org/10.5194/essd-13-515-2021

Borrelli, P., Robinson, D. A., Fleischer, L. R., Lugato, E., Ballabio, C., Alewell, C., et al. (2017). An assessment of the global impact of 21st century land use change on soil erosion. *Nature Communications*, *8*(1), 2013. https://doi.org/10.1038/s41467-017-02142-7

Bouwman, A. F., Bierkens, M. F. P., Griffioen, J., Hefting, M. M., Middelburg, J. J., Middelkoop, H., & Slomp, C. P. (2013). Nutrient dynamics, transfer and retention along the aquatic continuum from land to ocean: Towards integration of ecological and biogeochemical models. *Biogeosciences*, *10*(1), 1–22. https://doi.org/10.5194/bg-10-1-2013

Bouwman, L., Goldewijk, K. K., Van Der Hoek, K. W., Beusen, A. H. W., Van Vuuren, D. P., Willems, J., et al. (2013). Exploring global changes in nitrogen and phosphorus cycles in agriculture induced by livestock production over the 1900-2050 period. *Proceedings of the National Academy of Sciences of the United States of America*, *110*(52), 20882–20887. https://doi.org/10.1073/pnas.1012878108

Carpenter, S. R. (2005). Eutrophication of aquatic ecosystems: Bistability and soil phosphorus. *Proceedings of the National Academy of Sciences of the United States of America*, *102*(29), 10002–10005. https://doi.org/10.1073/pnas.0503959102

Carpenter, S. R., & Bennett, E. M. (2011). Reconsideration of the planetary boundary for phosphorus. *Environmental Research Letters*, *6*(1), 014009. https://doi.org/10.1088/1748-9326/6/1/014009

Carpenter, S. R., Booth, E. G., & Kucharik, C. J. (2018). Extreme precipitation and phosphorus loads from two agricultural watersheds. *Limnology & Oceanography*, *63*(3), 1221–1233. https://doi.org/10.1002/lno.10767

Chapra, S. C. (2008). *Surface water-quality modeling*. Waveland press.

Chow, V. T. (2010). *Applied hydrology*. Tata McGraw-Hill Education.

Colborne, S. F., Maguire, T. J., Mayer, B., Nightingale, M., Enns, G. E., Fisk, A. T., et al. (2019). Water and sediment as sources of phosphate in aquatic ecosystems: The Detroit River and its role in the Laurentian Great Lakes. *The Science of the Total Environment*, *647*, 1594–1603. https://doi.org/10.1016/j.scitotenv.2018.08.029

Cole, T. M., & Wells, S. A. (2006). *CE-QUAL-W2: A two-dimensional, laterally averaged, hydrodynamic and water quality model*, version 3.5.

Compton, J., Mallinson, D., Glenn, C. R., Filippelli, G., Föllmi, K., Shields, G., & Zanin, Y. (2000). *Variations in the global phosphorus cycle*.

Conley, D. J., Paerl, H. W., Howarth, R. W., Boesch, D. F., Seitzinger, S. P., Havens, K. E., et al. (2009). Controlling eutrophication: Nitrogen and phosphorus. *Science*, *323*(5917), 1014–1015. https://doi.org/10.1126/science.1167755

Cordell, D., Drangert, J.-O., & White, S. (2009). The story of phosphorus: Global food security and food for thought. *Global Environmental Change*, *19*(2), 292–305. https://doi.org/10.1016/j.gloenvcha.2008.10.009

Correll, D. L. (1998). The role of phosphorus in the eutrophication of receiving waters: A review. *Journal of Environmental Quality*, *27*(2), 261–266. https://doi.org/10.2134/jeq1998.00472425002700020004x

Debele, B., Srinivasan, R., & Parlange, J.-Y. (2008). Coupling upland watershed and downstream waterbody hydrodynamic and water quality models (SWAT and CE-QUAL-W2) for better water resources management in complex river basins. *Environmental Modeling & Assessment*, *13*(1), 135–153. https://doi.org/10.1007/s10666-006-9075-1

Elser, J., & Bennett, E. (2011). A broken biogeochemical cycle. *Nature*, *478*(7367), 29–31. https://doi.org/10.1038/478029a

Enríquez, S., Duarte, C. M., & Sand-Jensen, K. A. J. (1993). Patterns in decomposition rates among photosynthetic organisms: The importance of detritus C: N: P content. *Oecologia*, *94*(4), 457–471. https://doi.org/10.1007/bf00566960

Fennel, K., & Laurent, A. (2018). N and P as ultimate and proximate limiting nutrients in the northern Gulf of Mexico: Implications for hypoxia reduction strategies. *Biogeosciences*, *15*(10), 3121–3131. https://doi.org/10.5194/bg-15-3121-2018

Garnier, J., Lassaletta, L., Billen, G., Romero, E., Grizzetti, B., Némery, J., et al. (2015). Phosphorus budget in the water-agro-food system at nested scales in two contrasted regions of the world (ASEAN-8 and EU-27). *Global Biogeochemical Cycles*, *29*(9), 1348–1368. https://doi.org/10.1002/2015gb005147

Goll, D. S., Moosdorf, N., Hartmann, J., & Brovkin, V. (2014). Climate-driven changes in chemical weathering and associated phosphorus release since 1850: Implications for the land carbon balance. *Geophysical Research Letters*, *41*(10), 3553–3558. https://doi.org/10.1002/2014GL059471

Goll, D. S., Vuichard, N., Maignan, F., Jornet-Puig, A., Sardans, J., Violette, A., et al. (2017). A representation of the phosphorus cycle for ORCHIDEE (revision 4520). *Geoscientific Model Development*, *10*(10), 3745–3770. https://doi.org/10.5194/gmd-10-3745-2017

Gu, A. Z., Liu, L., Neethling, J. B., Stensel, H. D., & Murthy, S. (2011). Treatability and fate of various phosphorus fractions in different wastewater treatment processes. *Water Science and Technology*, *63*(4), 804–810. https://doi.org/10.2166/wst.2011.312

Hale, R. L., Grimm, N. B., Vörösmarty, C. J., & Fekete, B. (2015). Nitrogen and phosphorus fluxes from watersheds of the northeast U.S. from 1930 to 2000: Role of anthropogenic nutrient inputs, infrastructure, and runoff. *Global Biogeochemical Cycles*, *29*(3), 341–356. https://doi.org/10.1002/2014GB004909

Harrison, J. A., Beusen, A. H., Fink, G., Tang, T., Strokal, M., Bouwman, A. F., et al. (2019). Modeling phosphorus in rivers at the global scale: Recent successes, remaining challenges, and near-term opportunities. *Current Opinion in Environmental Sustainability*, *36*, 68–77. https://doi.org/10.1016/j.cosust.2018.10.010

Hassan, M. A., Roberge, L., Church, M., More, M., Donner, S. D., Leach, J., & Ali, K. F. (2017). What are the contemporary sources of sediment in the Mississippi River? *Geophysical Research Letters*, *44*(17), 8919–8924. https://doi.org/10.1002/2017gl074046

Heidel, K., Roy, S., Creager, C., Chung, C.-F., & Grieb, T. (2006). *Conceptual model for nutrients in the central valley and Sacramento-San Joaquin Delta*. https://doi.org/10.13140/RG.2.2.13466.13769

Hirsch, R. M., Moyer, D. L., & Archfield, S. A. (2010). Weighted Regressions on time, discharge, and season (WRTDS), with an application to Chesapeake Bay river inputs. *Journal of the American Water Resources Association*, *46*(5), 857–880. https://doi.org/10.1111/j.1752-1688.2010.00482.x

Homer, C., Dewitz, J., Yang, L., Jin, S., Danielson, P., Xian, G., et al. (2015). Completion of the 2011 National Land Cover Database for the conterminous United States–representing a decade of land cover change information. *Photogrammetric Engineering & Remote Sensing*, *81*(5), 345–354.

Hu, M., Liu, Y., Zhang, Y., Shen, H., Yao, M., Dahlgren, R. A., & Chen, D. (2020). Long-term (1980–2015) changes in net anthropogenic phosphorus inputs and riverine phosphorus export in the Yangtze River basin. *Water Research*, *177*, 115779. https://doi.org/10.1016/j.watres.2020.115779

Jennings, E., Allott, N., Pierson, D. C., Schneiderman, E. M., Lenihan, D., Samuelsson, P., & Taylor, D. (2009). Impacts of climate change on phosphorus loading from a grassland catchment: Implications for future management. *Water Research*, *43*(17), 4316–4326. https://doi.org/10.1016/j.watres.2009.06.032

Jolliff, J. K., Kindle, J. C., Shulman, I., Penta, B., Friedrichs, M. A., Helber, R., & Arnone, R. A. (2009). Summary diagrams for coupled hydrodynamic-ecosystem model skill assessment. *Journal of Marine Systems*, *76*(1–2), 64–82. https://doi.org/10.1016/j.jmarsys.2008.05.014

Joos, F., & Spahni, R. (2008). Rates of change in natural and anthropogenic radiative forcing over the past 20, 000 years. *Proceedings of the National Academy of Sciences of the United States of America*, *105*(5), 1425–1430. https://doi.org/10.1073/pnas.0707386105

Kätterer, T., Reichstein, M., Andrén, O., & Lomander, A. (1998). Temperature dependence of organic matter decomposition: A critical review using literature data analyzed with different models. *Biology and Fertility of Soils*, *27*(3), 258–262. https://doi.org/10.1007/s003740050430

Kleinman, P., Sharpley, A., Buda, A., McDowell, R., & Allen, A. (2011). Soil controls of phosphorus in runoff: Management barriers and opportunities. *Canadian Journal of Soil Science*, *91*(3), 329–338. https://doi.org/10.4141/cjss09106

Koehler, B., von Wachenfeldt, E., Kothawala, D., & Tranvik, L. J. (2012). Reactivity continuum of dissolved organic carbon decomposition in lake water. *Journal of Geophysical Research*, *117*(G1). https://doi.org/10.1029/2011jg001793

Lee, C. J., Murphy, J. C., Crawford, C. G., & Deacon, J. R. (2017). *Methods for computing water-quality loads at sites in the U.S. Geological survey national water quality network* (Vol. 2017-1120). U.S. Geological Survey. (USGS Numbered Series No. 2017–1120). https://doi.org/10.3133/ofr20171120

Lewis, W. M., Jr. (2011). Global primary production of lakes: 19th baldi memorial lecture. *Inland Waters*, *1*(1), 1–28. https://doi.org/10.5268/iw-1.1.384

Li, H., Leung, L. R., Getirana, A., Huang, M., Wu, H., Xu, Y., et al. (2015). Evaluating global streamflow simulations by a physically based routing model coupled with the community land model. *Journal of Hydrometeorology*, *16*(2), 948–971. https://doi.org/10.1175/jhm-d-14-0079.1

Li, H., Wigmosta, M. S., Wu, H., Huang, M., Ke, Y., Coleman, A. M., & Leung, L. R. (2013). A physically based runoff routing model for land surface and Earth system models. *Journal of Hydrometeorology*, *14*(3), 808–828. https://doi.org/10.1175/jhm-d-12-015.1

Li, T., Wang, S., Liu, Y., Fu, B., & Zhao, W. (2020). A retrospective analysis on changes in sediment flux in the Mississippi river system: Trends, driving forces, and implications. *Journal of Soils and Sediments*, *20*(3), 1719–1729. https://doi.org/10.1007/s11368-019-02495-0

Li, Z., & Fang, H. (2016). Impacts of climate change on water erosion: A review. *Earth-Science Reviews*, *163*, 94–117. https://doi.org/10.1016/j.earscirev.2016.10.004

Litke, D. W. (1999). *Review of Phosphorus Control Measures in the United States and Their Effects on Water Quality* (Vol. 99). US Department of the Interior, US Geological Survey.

Liu, M., Tian, H., Yang, Q., Yang, J., Song, X., Lohrenz, S. E., & Cai, W.-J. (2013). Long-term trends in evapotranspiration and runoff over the drainage basins of the Gulf of Mexico during 1901–2008. *Water Resources Research*, *49*(4), 1988–2012. https://doi.org/10.1002/wrcr.20180

Lohrenz, S. E., Redalje, D. G., Cai, W.-J., Acker, J., & Dagg, M. (2008). A retrospective analysis of nutrients and phytoplankton productivity in the Mississippi River plume. *Continental Shelf Research*, *28*(12), 1466–1475. https://doi.org/10.1016/j.csr.2007.06.019

Lu, C., Zhang, J., Tian, H., Crumpton, W. G., Helmers, M. J., Cai, W.-J., et al. (2020). Increased extreme precipitation challenges nitrogen load management to the Gulf of Mexico. *Communications Earth & Environment*, *1*(1), 1–10. https://doi.org/10.1038/s43247-020-00020-7

Maavara, T., Lauerwald, R., Regnier, P., & Van Cappellen, P. (2017). Global perturbation of organic carbon cycling by river damming. *Nature Communications*, *8*(1), 15347. https://doi.org/10.1038/ncomms15347

Maavara, T., Parsons, C. T., Ridenour, C., Stojanovic, S., Dürr, H. H., Powley, H. R., & Van Cappellen, P. (2015). Global phosphorus retention by river damming. *Proceedings of the National Academy of Sciences*, *112*(51), 15603–15608. https://doi.org/10.1073/pnas.1511797112

MacDonald, G. K., Bennett, E. M., & Carpenter, S. R. (2012). Embodied phosphorus and the global connections of United States agriculture. *Environmental Research Letters*, *7*(4), 044024. https://doi.org/10.1088/1748-9326/7/4/044024

MacDonald, G. K., Bennett, E. M., Potter, P. A., & Ramankutty, N. (2011). Agronomic phosphorus imbalances across the world's croplands. *Proceedings of the National Academy of Sciences*, *108*(7), 3086–3091. https://doi.org/10.1073/pnas.1010808108

Mahowald, N., Jickells, T. D., Baker, A. R., Artaxo, P., Benitez-Nelson, C. R., Bergametti, G., et al. (2008). Global distribution of atmospheric phosphorus sources, concentrations and deposition rates, and anthropogenic impacts: Global atmospheric phosphorus. *Global Biogeochemical Cycles*, *22*(4). https://doi.org/10.1029/2008GB003240

McDowell, R. W., Biggs, B. J. F., Sharpley, A. N., & Nguyen, L. (2004). Connecting phosphorus loss from agricultural landscapes to surface water quality. *Chemistry and Ecology*, *20*(1), 1–40. https://doi.org/10.1080/02757540310001626092

McGechan, M. B., & Lewis, D. R. (2002). SW—soil and water. *Biosystems Engineering*, *82*(1), 1–24. https://doi.org/10.1006/bioe.2002.0054

Meade, R. H., & Moody, J. A. (2010). Causes for the decline of suspended-sediment discharge in the Mississippi River system, 1940–2007. *Hydrological Processes*, *24*(1), 35–49. https://doi.org/10.1002/hyp.7477

Metson, G. S., Lin, J., Harrison, J. A., & Compton, J. E. (2017). Linking terrestrial phosphorus inputs to riverine export across the United States. *Water Research*, *124*, 177–191. https://doi.org/10.1016/j.watres.2017.07.037

Morée, A. L., Beusen, A. H. W., Bouwman, A. F., & Willems, W. J. (2013). Exploring global nitrogen and phosphorus flows in urban wastes during the twentieth century. *Global Biogeochemical Cycles*, *27*(3), 836–846. https://doi.org/10.1002/gbc.20072

Neitsch, S. L., Arnold, J. G., Kiniry, J. R., & Williams, J. R. (2011). *Soil and water assessment tool theoretical documentation version 2009*. Texas Water Resources Institute.

Pan, S., Bian, Z., Tian, H., Yao, Y., Najjar, R. G., Friedrichs, M. A. M., et al. (2021). Impacts of multiple environmental changes on long-term nitrogen loading from the Chesapeake Bay watershed. *Journal of Geophysical Research: Biogeosciences*, *126*(5), e2020JG005826. https://doi.org/10.1029/2020JG005826

Pan, S., Tian, H., Dangal, S. R., Ouyang, Z., Lu, C., Yang, J., et al. (2015). Impacts of climate variability and extremes on global net primary production in the first decade of the 21st century. *Journal of Geographical Sciences*, *25*(9), 1027–1044. https://doi.org/10.1007/s11442-015-1217-4

Pan, S., Yang, J., Tian, H., Shi, H., Chang, J., Ciais, P., et al. (2020). Climate extreme versus carbon extreme: Responses of terrestrial carbon fluxes to temperature and precipitation. *Journal of Geophysical Research: Biogeosciences*, *125*(4), e2019JG005252. https://doi.org/10.1029/2019JG005252

Pulley, S., Foster, I., & Antunes, P. (2016). The dynamics of sediment-associated contaminants over a transition from drought to multiple flood events in a lowland UK catchment. *Hydrological Processes*, *30*(5), 704–719. https://doi.org/10.1002/hyp.10616

Quinton, J. N., Govers, G., Van Oost, K., & Bardgett, R. D. (2010). The impact of agricultural soil erosion on biogeochemical cycling. *Nature Geoscience*, *3*(5), 311–314. https://doi.org/10.1038/ngeo838

Remo, J., Ryherd, J. K., Ruffner, C., & Therrell, M. (2017). *Temporal and spatial patterns of sedimentation within the batture lands of the middle Mississippi River*. https://doi.org/10.1016/J.GEOMORPH.2018.02.010

Ren, W., Tian, H., Cai, W.-J., Lohrenz, S. E., Hopkinson, C. S., Huang, W.-J., et al. (2016). Century-long increasing trend and variability of dissolved organic carbon export from the Mississippi River basin driven by natural and anthropogenic forcing: Export of DOC from the Mississippi River. *Global Biogeochemical Cycles*, *30*(9), 1288–1299. https://doi.org/10.1002/2016GB005395

Reynolds, C. S. (2006). *The ecology of phytoplankton*. Cambridge University Press.

Robson, B. J. (2014). State of the art in modelling of phosphorus in aquatic systems: Review, criticisms and commentary. *Environmental Modelling & Software*, *61*, 339–359. https://doi.org/10.1016/j.envsoft.2014.01.012

Rowe, H., Withers, P. J. A., Baas, P., Chan, N. I., Doody, D., Holiman, J., et al. (2016). Integrating legacy soil phosphorus into sustainable nutrient management strategies for future food, bioenergy and water security. *Nutrient Cycling in Agroecosystems*, *104*(3), 393–412. https://doi.org/10.1007/s10705-015-9726-1

Ruttenberg, K. C. (2003). The global phosphorus cycle. *TrGeo*, *8*, 682.

Ryther, J. H., & Dunstan, W. M. (1971). Nitrogen, phosphorus, and eutrophication in the coastal marine environment. *Science*, *171*(3975), 1008–1013. https://doi.org/10.1126/science.171.3975.1008

Sabo, R. D., Clark, C. M., Gibbs, D. A., Metson, G. S., Todd, M. J., LeDuc, S. D., et al. (2021). Phosphorus inventory for the conterminous United States (2002–2012). *Journal of Geophysical Research: Biogeosciences*, *126*(4), e2020JG005684. https://doi.org/10.1029/2020JG005684

Scavia, D., & Donnelly, K. A. (2007). Reassessing hypoxia forecasts for the Gulf of Mexico. *Environmental Science & Technology*, *41*(23), 8111–8117. https://doi.org/10.1021/es0714235

Sharpley, A., Jarvie, H. P., Buda, A., May, L., Spears, B., & Kleinman, P. (2013). Phosphorus legacy: Overcoming the effects of past management practices to mitigate future water quality impairment. *Journal of Environmental Quality*, *42*(5), 1308–1326. https://doi.org/10.2134/jeq2013.03.0098

Smil, V. (2000). Phosphorus in the environment: Natural flows and human interferences. *Annual Review of Energy and the Environment*, *25*(1), 53–88. https://doi.org/10.1146/annurev.energy.25.1.53

Sohrt, J., Lang, F., & Weiler, M. (2017). Quantifying components of the phosphorus cycle in temperate forests. *Wires Water*, *4*(6), e1243. https://doi.org/10.1002/wat2.1243

Stackpoole, S., Sabo, R., Falcone, J., & Sprague, L. (2021). Long-term Mississippi river trends expose shifts in the river load response to watershed nutrient balances between 1975 and 2017. *Water Resources Research*, *57*(11), e2021WR030318. https://doi.org/10.1029/2021WR030318

Stępień, I. (1984). On the numerical solution of the Saint-Vénant equations. *Journal of Hydrology*, *67*(1), 1–11. https://doi.org/10.1016/0022-1694(84)90228-2

Swaney, D. P., & Howarth, R. W. (2019). Phosphorus use efficiency and crop production: Patterns of regional variation in the United States, 1987–2012. *The Science of the Total Environment*, *685*, 174–188. https://doi.org/10.1016/j.scitotenv.2019.05.228

Sylvan, J. B., Dortch, Q., Nelson, D. M., Maier Brown, A. F., Morrison, W., & Ammerman, J. W. (2006). Phosphorus limits phytoplankton growth on the Louisiana shelf during the period of hypoxia formation. *Environmental Science & Technology*, *40*(24), 7548–7553. https://doi.org/10.1021/es061417t

Sylvan, J. B., Quigg, A., Tozzi, S., & Ammerman, J. W. (2007). Eutrophication-induced phosphorus limitation in the Mississippi River plume: Evidence from fast repetition rate fluorometry. *Limnology & Oceanography*, *52*(6), 2679–2685. https://doi.org/10.4319/lo.2007.52.6.2679

Tan, Z., Leung, L. R., Li, H.-Y., Tesfa, T., Zhu, Q., Yang, X., et al. (2021). Increased extreme rains intensify erosional nitrogen and phosphorus fluxes to the northern Gulf of Mexico in recent decades. *Environmental Research Letters*, *16*(5), 054080. https://doi.org/10.1088/1748-9326/abf006

Tao, B., Tian, H., Ren, W., Yang, J., Yang, Q., He, R., et al. (2014). Increasing Mississippi river discharge throughout the 21st century influenced by changes in climate, land use, and atmospheric CO_2: Factorial analyses OF river discharge. *Geophysical Research Letters*, *41*(14), 4978–4986. https://doi.org/10.1002/2014GL060361

Terrer, C., Jackson, R. B., Prentice, I. C., Keenan, T. F., Kaiser, C., Vicca, S., et al. (2019). Nitrogen and phosphorus constrain the CO 2 fertilization of global plant biomass. *Nature Climate Change*, *9*(9), 684–689. https://doi.org/10.1038/s41558-019-0545-2

Tesfa, T. K., Leung, L. R., Huang, M., Li, H.-Y., Voisin, N., & Wigmosta, M. S. (2014). Scalability of grid- and subbasin-based land surface modeling approaches for hydrologic simulations. *Journal of Geophysical Research: Atmospheres*, *119*(6), 3166–3184. https://doi.org/10.1002/2013JD020493

Thomann, R. V., & Mueller, J. A. (1987). *Principles of surface water quality modeling and control*. Harper & Row Publishers.

Tian, H., Chen, G., Liu, M., Zhang, C., Sun, G., Lu, C., et al. (2010). Model estimates of net primary productivity, evapotranspiration, and water use efficiency in the terrestrial ecosystems of the southern United States during 1895–2007. *Forest Ecology and Management*, *259*(7), 1311–1327. https://doi.org/10.1016/j.foreco.2009.10.009

Tian, H., Chen, G., Lu, C., Xu, X., Hayes, D. J., Ren, W., et al. (2015). North American terrestrial CO2 uptake largely offset by CH4 and N2O emissions: Toward a full accounting of the greenhouse gas budget. *Climatic Change*, *129*(3), 413–426. https://doi.org/10.1007/s10584-014-1072-9

Tian, H., Ren, W., Yang, J., Tao, B., Cai, W.-J., Lohrenz, S. E., et al. (2015). Climate extremes dominating seasonal and interannual variations in carbon export from the Mississippi River Basin. *Global Biogeochemical Cycles*, *29*(9), 1333–1347. https://doi.org/10.1002/2014GB005068

Tian, H., Xu, R., Pan, S., Yao, Y., Bian, Z., Cai, W.-J., et al. (2020). Long-term trajectory of nitrogen loading and delivery from Mississippi River basin to the Gulf of Mexico. *Global Biogeochemical Cycles*, *34*(5), e2019GB006475. https://doi.org/10.1029/2019GB006475

Tiessen, H., Salcedo, I. H., & Sampaio, E. (1992). Nutrient and soil organic matter dynamics under shifting cultivation in semi-arid northeastern Brazil. *Agriculture, Ecosystems & Environment*, *38*(3), 139–151. https://doi.org/10.1016/0167-8809(92)90139-3

Turner, R. E., & Rabalais, N. N. (2003). Linking landscape and water quality in the Mississippi River basin for 200 years. *BioScience*, *53*(6), 563–572. https://doi.org/10.1641/0006-3568(2003)053[0563:LLAWQI]2.0.CO;2

van der Zee, S., Leus, F., & Louer, M. (1989). Prediction of phosphate transport in small columns with an approximate sorption kinetics model. *Water Resources Research*, *25*(6), 1353–1365. https://doi.org/10.1029/WR025i006p01353

Van Drecht, G., Bouwman, A. F., Harrison, J., & Knoop, J. M. (2009). Global nitrogen and phosphate in urban wastewater for the period 1970 to 2050. *Global Biogeochemical Cycles*, *23*(4). https://doi.org/10.1029/2009GB003458

van Puijenbroek, P. J. T. M., Beusen, A. H. W., & Bouwman, A. F. (2019). Global nitrogen and phosphorus in urban waste water based on the Shared Socio-economic pathways. *Journal of Environmental Management*, *231*, 446–456. https://doi.org/10.1016/j.jenvman.2018.10.048

Vilmin, L., Aissa-Grouz, N., Garnier, J., Billen, G., Mouchel, J.-M., Poulin, M., & Flipo, N. (2015). Impact of hydro-sedimentary processes on the dynamics of soluble reactive phosphorus in the Seine River. *Biogeochemistry*, *122*(2), 229–251. https://doi.org/10.1007/s10533-014-0038-3

Viovy, N. (2018). CRUNCEP version 7 - atmospheric forcing data for the community land model [Data set]. UCAR/NCAR - Research Data Archive. https://doi.org/10.5065/PZ8F-F017

Wang, Z., Tian, H., Yang, J., Shi, H., Pan, S., Yao, Y., et al. (2020). Coupling of phosphorus processes with carbon and nitrogen cycles in the dynamic land ecosystem model: Model structure, parameterization, and evaluation in tropical forests. *Journal of Advances in Modeling Earth Systems*, *12*(10), e2020MS002123. https://doi.org/10.1029/2020MS002123

Williams, J. R. (1995). The EPIC model. *Computer Models of Watershed Hydrology*, 909–1000.

Wu, H., Kimball, J. S., Li, H., Huang, M., Leung, L. R., & Adler, R. F. (2012). A new global river network database for macroscale hydrologic modeling. *Water Resources Research*, *48*(9), 2012WR012313. https://doi.org/10.1029/2012WR012313

Yamazaki, D., O'Loughlin, F., Trigg, M. A., Miller, Z. F., Pavelsky, T. M., & Bates, P. D. (2014). Development of the global width database for large rivers. *Water Resources Research*, *50*(4), 3467–3480. https://doi.org/10.1002/2013WR014664

Yang, X., Post, W. M., Thornton, P. E., & Jain, A. (2013). The distribution of soil phosphorus for global biogeochemical modeling. *Biogeosciences*, *10*(4), 2525–2537. https://doi.org/10.5194/bg-10-2525-2013

Yao, Y., Tian, H., Pan, S., Najjar, R. G., Friedrichs, M. A. M., Bian, Z., et al. (2021). Riverine carbon cycling over the past century in the mid-Atlantic region of the United States. *Journal of Geophysical Research: Biogeosciences*, *126*(5), e2020JG005968. https://doi.org/10.1029/2020JG005968

Yao, Y., Tian, H., Shi, H., Pan, S., Xu, R., Pan, N., & Canadell, J. G. (2020). Increased global nitrous oxide emissions from streams and rivers in the Anthropocene. *Nature Climate Change*, *10*(2), 138–142. https://doi.org/10.1038/s41558-019-0665-8

Yu, Z., & Lu, C. (2018). Historical cropland expansion and abandonment in the continental U.S. during 1850 to 2016. *Global Ecology and Biogeography*, *27*(3), 322–333. https://doi.org/10.1111/geb.12697